Title

SMALL ATOM APPROXIMATIONS FOR PHOTOELECTRON SCATTERING IN TEE INTERMEDIATE ENERGY RANGE

Authors

Barton, J.J.
Shirley, D.A.

Publication Date

1985-03-01

Lawrence Berkeley Laboratory
UNIVERSITY OF CALIFORNIA

Materials & Molecular Research Division

Submitted to The Physical Review, B

SMALL ATOM APPROXIMATIONS FOR PHOTOELECTRON SCATTERING IN THE INTERMEDIATE ENERGY RANGE

J.J. Barton and D.A. Shirley

March 1985

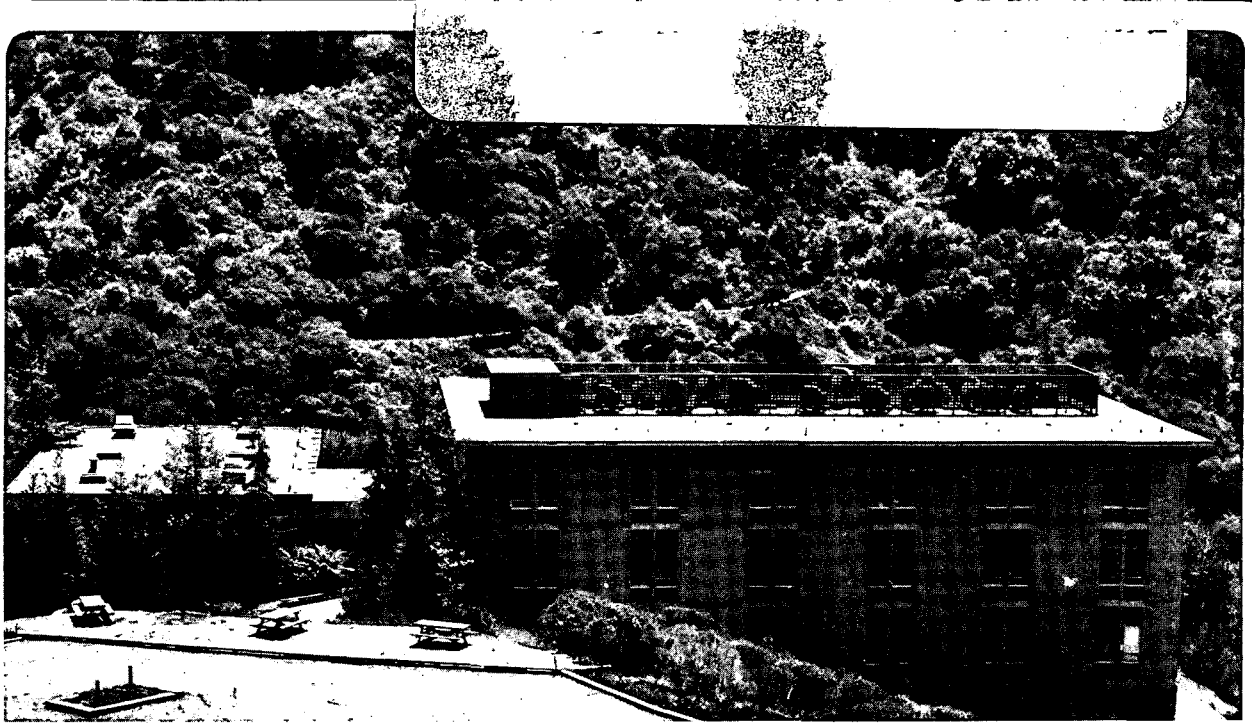

Prepared for the U.S. Department of Energy under Contract DE-AC03-76SF00098

DISCLAIMER

LBL-18693

SMALL ATOM APPROXIMATIONS FOR PHOTOELECTRON SCATTERING IN THE INTERMEDIATE ENERGY RANGE

J.J. Barton and D.A. Shirley

Materials and Molecular Research Division
Lawrence Berkeley Laboratory
and
Department of Chemistry
University of California
Berkeley, California 94720

ABSTRACT

Five approximate models for describing the scattering of spherical waves by central potentials are explored. The point-scattering model introduced by Lee and Pendry (Phys. Rev. B, 11,2795,(1975)) allows a short-range potential to be close to the source; a new homogeneous wave model lifts the restriction on the potential diameter, but requires asymptotic incident waves. The popular plane-wave model requires both an infinitesimal diameter potential and incident waves at their asymptotic limit. For realistic potentials at near-neighbor separations, none of these models is adequate: even a hybrid model combining features of the point-scattering and homogeneous-wave methods does not allow for amplitude variation across the potential. The fifth small atom model is based on a Taylor series, magnetic quantum number expansion of the addition theorem for screened spherical waves. This Taylor series approximation has the homogeneous-wave model as its zero-order term and the exact spherical wave scattering process as its limit.

Multiple-scattering equations for Angle-Resolved Photoemission Extended Fine Structure (ARPEFS) are derived and the effectiveness of these approximations are compared. We demonstrate that while the plane-wave model is reasonably accurate for near-180° backscattering, small angle scattering requires the curved wavefront corrections available in the Taylor series expansion method.

I. INTRODUCTION

The theoretical description of electron scattering in solids for intermediate energies from 100 to 1000 eV faces a peculiar challenge: simple physical models for the scattering process are surprisingly accurate, while more sophisticated calculations become intractable. The striking success of single-scattering, plane-wave models for the qualitative description of Angle-Resolved Photoemission Extended Fine Structure (ARPEFS)[1] and of Extended X-ray Absorption Fine Structure (EXAFS)[2] has led to satisfactory empirical analysis of these measurements, but multiple-scattering, spherical wave calculations are too complex for routine quantitative analysis cases where the simple model fails.

The two crucial theoretical issues--spherical vs. plane-wave scattering and multiple versus single scattering--are entwined. First, we must decide if the curvature of the wave emanating from one ion core will influence the scattering of that wave by an adjacent potential. If we may neglect the curvature, then the scattering of electrons in a solid reduces to a series of plane-wave calculations, connected only through the wave phase and incident direction.[3] If, on the other hand, the curvature is important, more sophisticated calculations are required. For single scattering of ℓ=1 photoelectrons we have previously derived the required equations.[4] Unfortunately the outgoing scattered wave from the first scattering event will always contain much higher angular momentum partial waves, requiring more sophisticated

equations and leading to larger corrections. Thus if double scattering is important, we certainly would expect the wave curvature to be important.

This leads us to the second central issue in electron scattering: the role of multiple scattering. The various experimental processes address different aspects of this issue. The results of Low Energy Electron Diffraction (LEED) calculations[5] are clear: multiple scattering is important. Theoretical work with photoelectron scattering[6] and more recent work on x-ray absorption edges[7] have utilized the relative simplicity of the photoelectron scattering process to show that at intermediate energies only forward scattering leads to multiple scattering events at a level that cannot be neglected. Finally in EXAFS the photoelectron returns to the absorbing atom: in the process a large number of high angular-momentum waves are backscattered to the absorber. Thus our previous conclusion that double scattering would require curved wave calculations is contradicted by evidence[8,9] that a plane-wave model contains the essential character of the EXAFS phenomenon; we might be further tempted to extrapolate the empirical evidence and ignore wavefront curvature for all scattering at high energy.[3] Any correct theoretical procedure must be compatible with all of these observations.

In a previous paper,[4] we explored the wavefront curvature question for single scattering of $\ell=1$ photoelectrons. Two important conclusions from that work are i) curved wave corrections are much smaller for backscattering than they are for forward scattering, and ii) only the backscattering corrections get smaller at high energy; the forward

scattering corrections do not fall asymptotically with large k. Because the studies cited above already demonstrate the importance of forward scattering, and because the once-scattered wave will contain angular momenta much greater than $\ell=1$, we are led to investigate curved wavefront corrections to multiple scattering in the intermediate energy range.

This would seem to be a rather straightforward project. We have after all an impressive foundation in the low energy region from LEED theory,[5] photoelectron diffraction[10], and, more recently, near edge x-ray absorption.[11] Indeed, Tong and co-workers have extended their photoelectron diffraction calculations into the intermediate energy range,[10] and their results have provided indications of the importance of multiple scattering. These calculations are not, however, simple extensions of the plane wave model; they are full curved-wave treatments and consequently--for a reason we now discuss--much more expensive than low energy multiple scattering calculations.

The origin of the difficulty in applying multiple scattering curved wave calculations at intermediate energies is that the maximum angular momentum in a scattered wave leaving a scattering atom <u>increases</u> with electron wavenumber. The maximum angular momentum, ℓ_{max}, scattering from a potential may be related to its range, r_0, by[12]

$$kr_o = \sqrt{\ell_{max}(\ell_{max}+1)} \approx \ell_{max}. \qquad (1)$$

As the energy--and hence the number of important scattered waves--increases, the number of numerical operations also increases. For plane-wave models this increase is manageable because each scattering event depends only linearly on ℓ_{max}. On the other hand, the time required for exact curved wave calculations are proportional to at least $(\ell_{max})^4$, prohibiting even exploratory multiple scattering calculations to be attempted. (Also note that approximate curved wave calculations based on a small, fixed maximum angular momentum will be incorrect above some energy given by eqn. (1)).

Simply from the success of plane-wave models of electron scattering we may conclude that another physical approximation must exist that would allow accurate introduction of curved wave corrections with more modest effort than the exact theory requires. In this paper we seek such an approximation by examining five approximate models for the scattering of spherical waves from central potentials:

i) point scattering,

ii) homogeneous wave scattering,

iii) plane-wave,

iv) renormalized homogeneous wave,

v) Taylor series-magnetic quantum number expansion.

The first four models were initially motivated by existing angular-momentum expansions known as addition theorems. We discuss the approximations necessary for each model and outline the physical problems to which they apply. The fifth small atom approximation is based on a new angular-momentum series expansion[13]; it contains

important curved wave corrections not included in any of the first four models and it provides for orderly development of higher order corrections.

In section II we discuss electron scattering of spherical waves by the partial wave method and exact scattering of spherical waves in the 100-1000 eV range. Physically motivated small atom approximations to the spherical wave formula are reviewed in section III, and we examine some of the contributions to the success of the plane-wave model. The remaining sections concern the fifth, more general small atom model. Section IV applies the Taylor series expansion for the spherical wave scattering to (1s) initial state photoelectron scattering. Section V discusses spherical wave scattering factors which govern the convergence of the Taylor series and Section VI illustrates the convergence for a single example and describes an intuitive picture of the Taylor series terms. We conclude in section VII with some remarks on further applications.

II. SPHERICAL WAVE SCATTERING AND NOZAWA'S GAUNT INTEGRAL SUMMATION

To provide the background for our development of approximate electron scattering formulae, we will set up the electron scattering problem, review Nozawa's origin-shift addition theorem[14] for spherical waves, and discuss the difficulty with this approach.

Our scattering system consists of a point source of electrons and a lattice of non-overlapping central potentials (the muffin-tin model[5]). This model approximates a number of physical problems. If the lattice represents a surface system and the point source is a screened photoemitter, then we have a photoelectron diffraction or Angle-Resolved Photoemission Extended Fine Structure model. If the lattice is a bulk material or surface system, the point source is again a screened photoemitter, and we calculate an integrated photoabsorption cross section, then we have an Extended X-ray Absorption Fine Structure (EXAFS) model. If the lattice is a surface, but the point source is a once scattered electron from an incoming plane wave, we have part of a model for multiple scattering, Low Energy Electron Diffraction (a sum over all scattering potentials excited by the plane wave is required to complete the LEED problem). For numerical calculation and physical discussion, the photoelectron diffraction (ARPEFS) case is the simplest problem because the scattered wave is directly detected. We shall concentrate on this problem.

If we consider a model which consists of non-overlapping potentials, we may calculate the multiple scattering by combining a general description for a spherical wave scattering from a potential

with a prescription for enumerating all significant scattering paths. Because we wish to describe photoelectron diffraction in the intermediate energy range (ARPEFS), we will concentrate on the scattering of photoelectrons originating from a (1s) level of an atom in an ordered and oriented system. We will also choose our examples to correspond to a recent ARPEFS experiment[1] on the c(2x2)S/Ni(001) system.

When the angle-resolved cross section for S(1s) photoemission is measured in such a system, the intensity oscillates with energy demonstrating interference among channels describing the possible paths to the detector.[15] Most of the interference occurs between waves describing direct and single-scattered photoemission, but forward scattering of the single-scattered electrons must also be included to predict the interference amplitude correctly.[10] A more complete discussion of the physics of photoelectron diffraction can be obtained elsewhere.[6,15,16] For the purposes of this paper we note that:

i) dipole selection rules predict that a single p type (ℓ=1) continuum orbital is populated through photoabsorption by a (1s) initial orbital,

ii) by selecting the $\hat{z}$ axis of our coordinate system parallel to the electric vector of a polarized photon beam, the photoelectron angular distribution can be written as proportional to $Y_{10}(\hat{r}) = (3/4\pi)^{1/2}\cos\theta$,

iii) in most materials, the photoion may be considered fully screened on the absorbing atom, and

iv) both the photoabsorbing atom's phase shift of the continuum wave and the total atomic cross section appear equally in all terms describing the final amplitude and thus do not affect the oscillations. Thus the oscillations may be isolated by normalization to form a function $\chi(k)=I(k)/I_0(k)-1$ as in EXAFS, but $\chi(k)$ contains no source-atom phase shift, in contrast to EXAFS.

With these ideas in mind, we may write the important part of the outgoing wavefunction as an $\ell=1$ spherical wave

$$\psi_0(\hat{r}) = ih_1(kr)Y_{10}(\hat{r}) \qquad (2)$$

We refer to this wavefunction as the "direct" wave.

We will use the scattering geometry depicted in Figure 1. We use $\vec{r}$ as a general position vector, and $\vec{k}$ as the propagation vector of the electron, with k giving the electron wave number. We define the scattering potential positions by $\vec{a}$, $\vec{b}$, $\vec{c}$... for the first, second, third and so on, scattering events. These latter vectors connect atoms: they are "bond" vectors, not position vectors. The vector $\vec{R}$ is the position of the angle resolving detector. Our convention and notation for spherical harmonics, $Y_{\ell m}$, are given in Appendix A of ref 13. For brevity we use the notation $Y_{\ell m}(\hat{r})$, where $\hat{r} = \vec{r}/r$. The functions $j_\ell(kr)$ and $h_\ell(kr) = h_\ell^{(1)}(kr)$ are spherical Bessel functions as defined by, for example, Pendry[5], Appendix A.

Our discussion of the small atom approximations will consider the single and double scattering of ℓ=1 photoelectron waves. A single scattering event will have an incident ℓ=1 wave (eqn. (2)), but the second event in double scattering will include all angular momenta characteristic of the multiple scattering problem. Thus higher order scattering can be built up by repeating the steps in the second part of our double scattering equations.

To better understand the small atom models, we will first briefly review the potential scattering of plane and spherical waves. If a plane wave is incident upon the potential, the expansion in an angular momentum series is well known:

$$e^{i\vec{k}\cdot\vec{r}} = \sum_{\ell''m''} 4\pi\, i^{\ell''} j_{\ell''}(kb) Y_{\ell''m''}(\hat{b}) Y^{*}_{\ell''m''}(\hat{k}) \qquad (3)$$

where $\vec{k}=k\hat{a}$ and $\vec{r} = \vec{a} + \vec{b}$. The partial wave method[17] instructs us to expect an outgoing spherical wave, $i^{\ell} h_{\ell}(kr) Y_{\ell m}(kr)$, proportional to each regular spherical wave incident on the potential; the complex proportionality factor, T_{ℓ}, is derived from the partial wave phase shifts, $\delta_{\ell}(k)$, and has both a scattering amplitude and wave phase shift:

$$T_{\ell}(k) = i \sin \delta_{\ell}\, e^{i\delta_{\ell}} = \frac{1}{2}\left(e^{i2\delta_{\ell}(k)} - 1\right) \qquad (4)$$

Thus the scattered wave becomes

$$\psi_{\vec{a}}(\vec{b}) = \sum_{\ell''m''} 4\pi\, i^{\ell''} h_{\ell''}(kb) Y_{\ell''m''}(\hat{b}) T_{\ell''}(k) Y^{*}_{\ell''m''}(\hat{a}) \quad \text{(plane wave)} \qquad (5)$$

(We will subscript a scattered wave by its origin; for a wave at the detector we replace $\vec{b}$ by $\vec{R}$.).

If a spherical wave from a source at the origin is incident on the potential centered at $\vec{a}$, the expansion in spherical harmonics has been derived by Nozawa.[14] If the spherical wave emanates from the origin, we may expand it around $\vec{a}$ as

$$i^{\ell} h_{\ell}(kr) Y_{\ell m}(\hat{r}) = \sum_{\ell''m''} G_{\ell m \ell'' m''} i^{\ell''} j_{\ell''}(kb) Y_{\ell''m''}(\hat{b}) \qquad (6)$$

$$G_{\ell m \ell'' m''} = \sum_{\ell' m'} 4\pi\, i^{\ell'} h_{\ell'}(ka) Y^{*}_{\ell' m'}(\hat{a}) \int Y_{\ell m}(\hat{k}) Y_{\ell' m'}(\hat{k}) Y^{*}_{\ell'' m''}(\hat{k}) d\hat{k}$$

where $\vec{r}=\vec{a}+\vec{b}$. In the mathematical literature, this type of formula is called an addition theorem; we will refer to this equation as Nozawa's origin-shift addition theorem. With this result we can calculate the scattered wave as

$$\psi_{\vec{a}}(\vec{b}) = \sum_{\ell''m''} T_{\ell''}(k) G_{\ell m \ell'' m''} i^{\ell''} h_{\ell''}(kb) Y_{\ell''m''}(\hat{b}) \qquad (7)$$

where $G_{\ell m \ell'' m''}$ is given above.

To understand and use this formula we must compute the integral of three spherical harmonics, called the Gaunt integral.[18] This integral can be related to the 3j vector addition (Clebsch-Gordan) symbols[19] and

Gaunt has derived an analytic formula to calculate its value. The integral is non-zero only when

$$m'' = m + m', \quad |\ell''-\ell| \leq \ell' \leq \ell'' + \ell \qquad \ell' + \ell'' + \ell = \text{even} \qquad (8)$$

Pendry[5] gave a computer program to implement Gaunt's formula. Typically a table of these Gaunt integrals is consulted in actual calculations.

The complexity of the formula for spherical wave scattering is self-evident. In computer calculations we must recognize that the number of transformation coefficients $G_{\ell m \ell'' m''}$ is proportional to $(\ell_{max}+1)^4$ and each coefficient requires the summation of $\sim \ell_{max}$ complex numbers times the Gaunt integral. Since ℓ_{max} is roughly proportional to k, multiple scattering calculations already difficult at $k = 3\text{Å}^{-1}$ become prohibitively expensive at $k = 12\text{Å}^{-1}$. Even this presumes that the Gaunt integrals are calculated once and stored; for calculations to 600 eV ($\ell_{max} = 19$), $\sim 10^6$ integrals are required. For these reasons we must approximate the scattering calculations.

III. PHYSICALLY MOTIVATED SMALL ATOM APPROXIMATIONS

Faced with the intractable spherical wave equations we are led to consider approximate forms. In this section we will examine four approximations, which we will refer to as point scattering, homogeneous wave scattering, plane-wave scattering, and the hybrid, renormalized homogeneous wave method. In the point scattering model, the incident spherical wave is treated exactly, but the potential is taken to have an infinitesimal diameter. This model was introduced by Lee and Pendry[8] as a small atom approximation for EXAFS. The homogeneous wave model allows the potential to have a physical diameter but every incident wave is assumed to have reached its asymptotic limit, exp(ikr)/ikr. The plane-wave model is the common limit of both the point scattering and homogeneous wave models; it assumes an infinitesimal potential and incident waves at their asymptotic limit. The renormalized homogeneous wave model combines the mechanics of the point scattering and homogeneous wave methods. Figure 2 compares these approximations graphically for an $\ell=7$ spherical wave. We begin by deriving formulae for the scattered waves in each approximation.

A. Point Scattering Model

The motivation for the point scattering model is a practical one: the origin-shift addition theorem for plane waves, eqn. 3 is much simpler than the corresponding formula for spherical waves, eqn. 6. To repeat the physical approach of Lee and Pendry,[8] we imagine the outgoing spherical wave meeting a potential with a sufficiently small diameter so

that we may ignore the curvature of wavefronts across the potential and the change in wave amplitude and phase along the propagation direction in the region of the potential. In other words, we represent an incident spherical wave, $i^{\ell}h_{\ell}(kr)Y_{\ell m}(\hat{r})$, over the infinitesimal point potential by a plane wave with the amplitude and phase of the spherical wave

$$i^{\ell}h_{\ell}(kr)Y_{\ell m}(\hat{r}) \approx i^{\ell}h_{\ell}(ka)Y_{\ell m}(\hat{a})e^{ik\hat{a}\cdot(\vec{r}-\vec{a})} \tag{9}$$

For a potential of finite diameter, the point-scattering approximate wave will agree with the actual incident wave only at the point $\vec{a}$. As illustrated in figure 2(b), this alignment and the common asymptotic frequency of the exact and approximate waves leads to good agreement between these waves except near the edges of the potential.

We may expand the plane wave with eqn. 3 and use the partial wave prescription to derive the scattered wave as

$$\psi_{\vec{a}}(\vec{b}) \approx ih_1(ka)Y_{10}(\hat{a}) \sum_{\ell'm'} 4\pi\, T_{\ell',\vec{a}}(k)\, Y_{\ell'm'}(\hat{a})i^{\ell'}h_{\ell'}(kb)Y_{\ell'm'}(\hat{b} \tag{10}$$

for an incident $\ell=1$ photoelectron wave (eqn. (2)). The same procedure may be applied to the wave emanating from $\vec{a}$ and scattering from a point potential at $\vec{b}$ into the direction of $\vec{c}$ to give a double scattered wave:

$$\psi_{\vec{a}\vec{b}}(\vec{c}) \approx ih_1(ka)Y_{10}(\hat{a}) \sum_{\ell'm'} 4\pi\, T_{\ell',\vec{a}}(k)Y_{\ell'm'}(\hat{a})i^{\ell'}h_{\ell'}(kb)Y_{\ell'm'}(\hat{b})$$

$$\sum_{\ell''m''} 4\pi\, T_{\ell'',\vec{b}}(k) Y_{\ell''m''}(\hat{b}) i^{\ell''} h_{\ell''}(kc) Y_{\ell''m''}(\hat{c}) \tag{11}$$

It is useful to separate the spherical Hankel function into asymptotic and polynomial parts:

$$i^{\ell} h_{\ell}(kr) = \frac{e^{ikr}}{ikr}\, d_{\ell}(kr); \tag{12}$$

where $d_{\ell}(kr)$ is given by a series[20]:

$$d_{\ell}(kr) = \sum_{p=0}^{\ell} \frac{(\ell+p)!}{p!(\ell-p)!} \left(\frac{i}{2kr}\right)^{p} \tag{13}$$

or, for practical calculations, by a recursion formula:

$$d_{\ell+1}(kr) = d_{\ell-1}(kr) - \frac{(2\ell+1)}{ikr}\, d_{\ell}(kr); \quad d_0 = 1,\ d_1 = 1 + \frac{i}{kr}\ . \tag{14}$$

In the limit that $2kr >> \ell(\ell+1)$, $d_{\ell}(kr) = 1.0$. We further define a scattering factor

$$f_{ab}^{point} = \frac{1}{ik} \sum_{\ell} (2\ell+1)\, T_{\ell,\vec{a}}(k)\, d_{\ell}(kb)\, P_{\ell}(\cos\Theta_{ab}) \tag{15}$$

which together with the addition theorem for spherical harmonics:

$$4\pi \sum_{m} Y_{\ell m}(\hat{a}) Y^{*}_{\ell m}(\hat{b}) = (2\ell+1) P_{\ell}(\cos\Theta_{ab}) \tag{16}$$

allows us to write

$$\psi_a(\vec{b}) \approx d_1(ka)Y_{10}(\hat{a}) \frac{e^{ika}}{a} f_{ab}^{point} \frac{e^{ikb}}{ikb} \tag{17}$$

and

$$\psi_{ab}(\hat{c}) \approx d_\ell(ka)Y_{\ell m}(\hat{a}) \frac{e^{ika}}{a} f_{ab}^{point} \frac{e^{ikb}}{b} f_{bc}^{point} \frac{e^{ikr}}{ikr} \tag{18}$$

For a detector at a position $|\vec{R}| >> \ell_{max}/k$ the last point scattering factor will converge to the plane wave scattering factor of atomic physics:

$$f_{ab}^{plane} = \frac{1}{ik} \sum_{\ell} (2\ell+1)\, T_{\ell,\vec{a}}(k)\, P_\ell(\cos\Theta_{ab}) \tag{19}$$

and the single-scattered waves calculated at the detector will be

$$\psi_a(\vec{R}) \approx d_1(ka)Y_{10}(\hat{a}) \frac{e^{ika}}{a} f_{aR}^{plane} \frac{e^{ik|\vec{R}-\vec{a}|}}{ikR}, \tag{20}$$

and the double-scattered waves are

$$\psi_{ab}(\vec{R}) \approx d_1(ka)Y_{10}(\hat{a}) \frac{e^{ika}}{a} f_{ab}^{point} \frac{e^{ikb}}{b} f_{bR}^{plane} \frac{e^{ik|\vec{R}-\vec{a}-\vec{b}|}}{ikr}. \tag{21}$$

B. Homogeneous Wave Model.

The motivation and formulation of the homogeneous wave scattering model is similar to the point scattering method. The idea is to approximate the incident wave over the region of a finite range potential. If we notice[19] that a spherical wave reaches to within 10 percent of its asymptotic amplitude when $kr \geq 2\ell$, and that the angular distribution of a spherical wave is nearly constant whenever it has a large amplitude, or conversely the angular distribution changes most rapidly near nodes where the amplitude is small, then we are led to approximate the spherical wave by its asymptotic limit, the isotropic spherical wave, $h_0(kr)$:

$$i^{\ell} h_{\ell}(kr) Y_{\ell m}(\hat{r}) \approx h_0(kr) Y_{\ell m}(\hat{a}) \tag{22}$$

Since $h_0(kr) = \exp(ikr)/ikr$, the homogeneous wave model explicitly incorporates the radial decay characteristic of spherical waves but allows no other variation in wave amplitude over the potential. In particular, the model ignores the amplitude variation of $Y_{\ell m}(\hat{r})$ laterally across the potential, the origin of our name "homogeneous wave" model. Thus the radial form of the incident wave is rather accurately approximated as shown in figure 2(c), but the waves are not in phase at the center of the potential. Although not shown by the radial plots in figure 2, the homogeneous wave model also incorporates the basic curvature characteristic of spherical waves. Thus the phase match between the homogeneous wave and the exact incident wave will appear as in figure 2(c) for any radial cut through the wave source, but

the match between the point scattering wave and the exact wave will be worse than figure 2(b) for any cut which does not pass through $\vec{a}$.

The isotropic spherical wave has a simple origin shift addition theorem similar to that of a plane wave:

$$h_0(kr) = \sum_{\ell''} (2\ell''+1) i^{\ell''} j_{\ell''}(kb) i^{\ell''} h_{\ell''}(ka) P_{\ell''}(\cos \Theta_{ab}) \tag{23}$$

and we may parallel the development of the point scattering equations with a different scattering factor

$$f_{ab}^{00} = \frac{1}{ik} \sum_{\ell''} (2\ell''+1)\ T_{\ell'',a}(k)\ d_{\ell''}(ka)\ P_{\ell''}(\cos \Theta_{ab}), \tag{24}$$

and arrive at the scattered wave amplitude at the detector in the homogeneous wave approximation

$$\psi_a(\vec{R}) = Y_{10}(\hat{a}) \frac{e^{ika}}{a} f_{aR}^{00} \frac{e^{ik|\vec{R}-\vec{a}|}}{ikR}, \tag{25}$$

and

$$\psi_{ab}(\vec{R}) = Y_{10}(\hat{a}) \frac{e^{ika}}{a} f_{ab}^{00} \frac{e^{ikb}}{b} f_{bR}^{00} \frac{e^{ik|\vec{R}-\vec{a}-\vec{b}|}}{ikR}. \tag{26}$$

(The superscript 00 is retained to parallel the notation of ref. 4). McDonnell, et al arrived at similar equations by an entirely different route in their original paper on Auger electron scattering[21].

C. Plane Wave Model.

Both the point-scattering and homogeneous wave models approach a plane-wave model for large scattering distances $|\vec{a}|$, but the distance at which these models reach the plane-wave limit depends on different parameters. In the point scattering model, the phase and amplitude differences between the spherical wave and a plane wave at the scattering point disappear as the $d_\ell(ka)$ approach 1.0. This requires $2ka >> \ell_{in}(\ell_{in}+1)$ where ℓ_{in} is the incident wave angular momentum. For homogeneous wave scattering we must move the potential far enough away to ignore the variation in 1/kr across the potential in the direction of propagation; this requires $2ka >> \ell_{out}(\ell_{out}+1)$ where ℓ_{out} is the outgoing wave angular momentum. (Note that these limiting criteria only specify the reduction of small atom approximations to the plane-wave limit; they are necessary but not sufficient conditions for plane-wave accuracy compared to the exact curved wave results). In the limit of either model the scattered waves at the detector become

$$\psi_a(\vec{R}) \approx Y_{10}(\hat{a}) \frac{e^{ika}}{a} f_{aR}^{plane} \frac{e^{ik|\vec{R}-\vec{a}|}}{ikR} \tag{27}$$

and

$$\psi_{ab}(\vec{R}) = Y_{10}(\hat{a}) \frac{e^{ika}}{a} f_{ab}^{plane} \frac{e^{ikb}}{b} f_{bR}^{plane} \frac{e^{ik|\vec{R}-\vec{a}-\vec{b}|}}{ikR} \tag{28}$$

It is this "plane-wave" form of the scattering equations that leads to the simple single scattering formulas for EXAFS[8] and ARPEFS.[15]

Neither the point scattering nor homogeneous wave models have persuasive advantages over the plane-wave limit in general scattering problems. Point scattering models the incident wave well at one point, without regard for the size of the potential. For point scattering to apply, we must be able to ignore the variation in 1/kr across the potential; from the homogeneous wave equations we can see this requires

$$2ka \gg \ell_{out}(\ell_{out}+1). \qquad (29)$$

Whenever this requirement is fulfilled, we have $2ka \gg \ell_{in}(\ell_{in}+1)$ for all $\ell_{in} \lesssim \ell_{out}$ and the plane-wave limit will be reached by the incident wave. In other words, only if we scatter high angular momentum waves off a short range potential where $\ell_{in} \gg \ell_{out}$ will point scattering significantly improve on the plane wave model. Roughly the converse is true for the homogeneous wave formulas. The homogeneous wave method considers the size of the potential, but approximates the incident wave. To ignore the difference in phase between the incident spherical wave and the isotropic homogeneous wave, $h_0(kr)$, we must have $\ell_{in}(\ell_{in}+1) \ll 2ka$. Whenever this requirement is fulfilled, we may ignore wave-front curvature for all $\ell_{out} \leq \ell_{in}$. Thus the homogeneous wave model will only improve on the plane-wave model for scattering low angular momentum waves from potentials with large effective radii, potentials which give rise to high angular momentum waves.

Despite these restrictions there are important problems to which these approximations apply. For the EXAFS single-scattering geometry, a

complete range of angular momentum waves are backscattered to the central atom, but only low angular momenta can couple through the dipole matrix element to the initial state; waves striking the central atom have $\ell_{in} >> \ell_{out}$. For the ARPEFS single-scattering problem, dipole excitation gives only low angular momentum waves for scattering and, since the high angular momentum waves only appear asymptotically, we have some cases of $\ell_{out} \geq \ell_{in}$. On the whole we might rank the homogeneous wave model ahead of the point scattering or plane-wave models more general scattering problems: low angular momentum partial waves carry much more weight when the scattered wave is constructed. We will also show in section IV that the homogeneous wave model is the zero order Taylor series term.

Our distinction between incident and outgoing angular momenta highlights the distinction - commonly overlooked - between the asymptotic limit of spherical Hankel functions and the plane wave limit of spherical waves. The asymptotic limit of $i^{\ell}h_{\ell}(kr)$ is $h_0(kr)=\exp(ikr)/ikr$ and we may invoke this limit whenever $2kr>>\ell(\ell+1)$. Even if the asymptotic limit is justified, the plane-wave limit may still fail to apply: the variation in (1/kr) across the potential may be significant if the potential has a large diameter. Conversely, the variation in (1/kr) may be neglected for a small diameter potential, but, if the incident angular momentum is high, we are not in the asymptotic limit of the spherical Hankel function. The plane-wave limit incorporates two approximations: the asymptotic limit and a negligible diameter potential.

D. Hybrid Model.

Our contention that the point scattering and homogeneous wave models have nearly opposite ranges of use would suggest a hybrid "renormalized" homogeneous wave method in which the phase and amplitude of the incident spherical wave is attached to the isotropic wave before scattering. Thus over the region of the potential we would represent the incident wave by

$$i^{\ell} h_{\ell}(kr) Y_{\ell m}(\hat{r}) \approx d_{\ell}(ka) Y_{\ell m}(\hat{a}) h_{o}(kr).$$

This approximation would agree with the incident wave in radial form (1/kr decay) and in phase and amplitude at $\vec{a}$ as shown in figure 2(d), and the phase agreement would extend to all points with $|\vec{r}| \approx |\vec{a}|$. While such a small atom approximation would give good results for the EXAFS and ARPEFS single scattering cases[22], we have no guarantee of success in multiple scattering problems: the criteria for the application of the small atom models we have examined thus far are necessary but not sufficient conditions for accuracy. The most serious limitation shared by these small atom approximations lies in directions not graphed in figure 2: none of the models described so far account for variation in wave amplitude across the potential due to the angular dependence of the spherical wave.

Rather than explore further the range of validity for these small atom approximations, we turn instead to the development of a new fifth approximation which allows steady improvement toward the exact curved-wave result. The development of this Taylor series, small atom approximation will comprise the following section; as a prelude we close

this section with two topics related to the plane-wave model. The first is simply the mathematical reduction of the exact origin-shift addition theorem, eqn. 6, to the plane wave limit; the required approximation bears upon our discussion above. Second, we attempt to understand the formally disconcerting but empirically well-founded success of the plane wave model, by listing several contributions to its usefulness.

E. Formal and Practical Plane-Wave Limits.

We may arrive at the plane-wave limit by replacing the spherical Hankel functions in Nozawa's origin-shift addition theorem by their asymptotic forms. We may then move the intermediate sum in equation 6 inside the Gaunt integral and, using the closure sum for spherical harmonics, perform the angle integration to conclude that

$$G_{\ell m \ell'' m''}(k\vec{a}) \sim 4\pi \frac{e^{ika}}{ika} Y_{\ell m}(\hat{a}) Y^{*}_{\ell'' m''}(\hat{a}) \qquad (30)$$

The addition theorem for spherical harmonics (eqn. 16) and the partial wave method then gives eqn. 27.

We may give the criterion for applying this approximation to Nozawa's origin-shift addition theorem as $\ell'(\ell'+1) << 2ka$ where ℓ' is the angular momentum of the intermediate sum in equation 6. The maximum intermediate angular momentum is restricted by the non-zero Gaunt integrals, eqn. 8, to be $\ell' = \ell'' + \ell$ or $\ell' = \ell_{in} + \ell_{out}$ using our notation from above. This sufficient condition for the plane-wave limit is much more restrictive than either conditions for the small atom

approximations and would indicate that plane-wave formulas would be adequate only for low angular momenta scattering from very short range potentials. We turn then to list some contribution to the success of the plane wave limit when 2ka is not much greater than $(\ell_{in} + \ell_{out})^2$.

Let us now try to understand the success of the plane wave method despite the evident theoretical problem. There are five important contributions:

i) The phase difference between the scattered wave and the unscattered wave is dominated by their different origins. Thus if we measure the phase difference between a backscattered wave and an unscattered wave, the phase calculated in the plane wave approximation need only be the same magnitude as that given by the spherical wave formula.[2]

ii) Spherical Hankel functions reach[19] to within 10 percent of their large kr limit when $kr \sim 2\ell_{max}$.

iii) At large k, the large number of contributing partial waves reduces the fractional error made in approximate treatment of the highest ℓ waves. In other words, the low ℓ waves have reached their asymptotic limit and the high ℓ waves become outnumbered.

iv) It has been discovered empirically from EXAFS analysis that the phase difference in the plane wave limit for backscattering may be reliably corrected by slight shifts in the scattering energy.[2] While discomforting from a

theoretical viewpoint, the scattering energy is not measured in the x-ray absorption experiment anyway.[23]

v) Finally, as discussed in reference 4, curved wave corrections are much smaller for backscattering due to cancellation of successive partial waves, or equivalently, as illustrated in figure 3, a smaller region of the potential contributes to backscattering.

Taken together, these ideas begin to explain the substantial success of the plane wave model. To make further progress in understanding the electron scattering or to enable efficient, accurate numerical calculation, especially for forward scattering directions, we must seek some approximation between the plane and full spherical wave formulas.

IV. TS-MQNE APPROXIMATION

To derive an approximate method beyond those discussed in the previous section we return to the exact Gaunt integral summation formula, eqn. 6, and ask how the known characteristics of the scattering problem might be used to eliminate physically unnecessary aspects of the mathematically exact origin-shift addition theorem. Any approximation scheme must recognize that we require an expansion with a particular form: it must be an angular momentum expansion about the potential center. Our solution is to expand the Fourier transform of the spherical wave in a Taylor series about the direction of the origin-shift vector, $\vec{a}$, translate the individual terms of the expansion, and obtain an angular momentum series when each term is subjected to the inverse Fourier transform. The result is a finite series capable of performing every duty of an origin-shift addition theorem, so we have reported its development separately[13]. The formula is

$$i^{\ell} h_{\ell}(kr) Y_{\ell m}(\hat{r}) = \sum_{q=-\ell}^{\ell} N_{\ell q} R^{(\ell)}_{qm}(0, \theta_{\varepsilon a}, \pi - \phi_{x\varepsilon a}) \sum_{p=0}^{\ell - |q|} C^{\ell}_{pq}$$

$$\sum_{\ell''=q}^{\infty} 4\pi i^{\ell''} j_{\ell''}(kr') Y_{\ell'' q}(\hat{r}') N_{\ell'' q} h_0(ka) H^{pq}_{\ell''}(ka) \qquad (31)$$

where $N_{\ell q}$ is a normalizing coefficient for spherical harmonics, $R^{(\ell)}_{qm}$ is a rotation matrix element[19], C^{ℓ}_{pq} contains factorials from the expansion of Legendre polynomials, and $H^{pq}_{\ell}(ka)$ may be expressed as an integral or

various series. The precise definition of the factors is given in ref. 13. This reference also describes an alternative view of the expansion in which the variable q is a magnetic quantum number in a coordinate system rotated to align the scattering and quantization axes. We will explore this magnetic quantum number expansion (MQNE) viewpoint in section V, but we will use the acronym now to refer to eqn. 31.

To calculate the wavefield due to scattering of the direct wave, eqn. 2, from a potential at a point $\vec{a}$, we first expand the direct wave about $\vec{a}$ using eqn. 31. For $\ell=1$, a first order Taylor expansion is exact:

$$ih_1(kr)Y_{10}(\hat{r}) = N_{10}R^{\ell}_{00}(0,\theta_{\varepsilon a},\pi-\phi_{x\varepsilon a}) \sum_{\ell} i^{\ell}j_{\ell}(kb)Y_{\ell 0}(\hat{b})N_{\ell 0}4\pi[H^{00}_{\ell}+H^{10}_{\ell}]$$

$$+ N_{11}R^{\ell}_{10}(0,\theta_{\varepsilon a},\pi-\phi_{x\varepsilon a}) \sum_{\ell} i^{\ell}j_{\ell}(kb)Y_{\ell 1}(\hat{b})N_{\ell-1}4\pi H^{01}_{\ell}$$

$$+ N_{1-1}R^{\ell}_{-10}(0,\theta_{\varepsilon a},\pi-\phi_{x\varepsilon a}) \sum_{\ell} i^{\ell}j_{\ell}(kb)Y_{\ell-1}(\hat{b})N_{\ell 1}4\pi H^{01}_{\ell} \qquad (32)$$

The rotation matrix elements are particularly simple when one of the subscripts is zero[19]:

$$R^{\ell}_{m0}(\alpha,\beta,\gamma) = \left(\frac{4\pi}{2\ell+1}\right)^{1/2} Y^{*}_{\ell m}(\beta,\alpha) \qquad (33)$$

Note all the magnetic sublevels here refer to the $\hat{a}$ axis (see ref 13, App. B). For $\ell=1$,

$$N_{10}R^{1}_{00}(0,\theta_{\varepsilon a},\pi-\phi_{x\varepsilon a}) = \left(\frac{3}{4\pi}\right)^{1/2} \cos\theta_{\varepsilon a} \tag{34}$$

and

$$N_{11}R^{1}_{10}(0,\theta_{\varepsilon a},\pi-\phi_{x\varepsilon a}) = N_{1-1}R^{1}_{-10}(0,\theta_{\varepsilon a},\pi-\phi_{x\varepsilon a}) = \frac{1}{2}\left(\frac{3}{4\pi}\right)^{1/2} \sin\theta_{\varepsilon a} \tag{35}$$

To calculate the scattered wave emanating from the potential at center $\hat{a}$, we replace $i^{\ell}j_{\ell}(kb)$ by $T_{\ell}(k)i^{\ell}h_{\ell}(kb)$ in the origin-shift formula. This single-scattered wave can then propagate to our detector or scatter again. We first consider the single-scattered wave at our detector.

For a detector at a position $|\vec{R}| >> |\vec{a}|$, the outgoing, scattered partial waves have all reached their asymptotic limit. As will be more apparent for the multiple scattering equations, it is convenient to define a new scattering factor

$$F^{00}_{pq}(k\vec{a},\hat{b}) = \frac{1}{ik}\sum_{\ell=|q|}(2\ell+1)\,T_{\ell}(k)\,H^{pq}_{\ell}\,P^{|q|}_{\ell}(\cos\theta_{ab})\,\frac{(\ell-|q|)!}{(\ell+|q|)!} \tag{36}$$

so that the single-scattered wave may be written

$$\psi_a(\vec{R}) = \left(\frac{3}{4\pi}\right)^{1/2}\frac{e^{ikR}}{ikR}\,\frac{e^{ika(1-\cos\theta_{aR})}}{a} \tag{37}$$

$$\{\cos\theta_{\varepsilon a}[F^{00}_{00}(k\vec{a},\hat{R}) + F^{00}_{10}(k\vec{a},\hat{R})] + \sin\theta_{\varepsilon a}\cos\phi_{\varepsilon aR}F^{00}_{01}(k\vec{a},\hat{R})\}$$

Reference 4 presents this same result in a different notation; Appendix A provides the connection.

Let us now return to the single-scattered wavefield near center $\vec{a}$ and tackle the multiple scattering case. The (exact) Taylor series origin shift, equation 32, and the partial wave phase shifts give the single-scattered wave in the near field region as

$$\psi_a(\vec{b}) = \frac{e^{ika}}{a} \sum_{q=-1}^{1} N_{1q} R^1_{q0}(0,\theta_{\varepsilon a},\pi-\phi_{x\varepsilon a}) \sum_{p=0}^{1-|q|} C^1_{pq}$$

$$\frac{1}{ik} \sum_{\ell=|q|} 4\pi\, T_{\ell,\vec{a}}(k)\, H^{pq}_{\ell}(ka)\, N_{\ell q}\, i^{\ell} h_{\ell}(kb) Y_{\ell q}(\hat{b}) \qquad (38)$$

The dependence on $\vec{b}$ in each term of this expansion is that of a spherical wave, $i^{\ell}h_{\ell}(kb)Y_{\ell q}(\hat{b})$, and as this wave encounters another potential at position $\vec{b}$, we can apply the MQNE formula and partial wave phase shifts again to calculate the double scattered wave. If we call $\psi^{\ell q}_{ab}(\vec{R})$ the wave generated when the (ℓ,q) spherical wave from $\vec{a}$ scatters from $\vec{b}$ and is detected at $\vec{R}$, then we have

$$\psi^{\ell q}_{ab}(\vec{R}) = \sum_{q'=-\ell}^{\ell} N_{\ell q} R^{\ell}_{q',q}(0,\theta_{ab},\pi-\phi_{\varepsilon ab}) \sum_{p'=0}^{\ell-|q'|} C^{\ell}_{p'q'}\, e^{iq'\phi_{abR}} \frac{e^{ikb}}{b} \frac{e^{ik|\vec{R}-\vec{a}-\vec{b}|}}{ik|\vec{R}-\vec{a}-\vec{b}|}$$

$$\left\{\frac{1}{ik} \sum_{\ell'=q'}^{\ell_{max}} (2\ell'+1)\, T_{\ell',\vec{b}}(k)\, H^{p'q'}_{\ell'}(kb)\, P^{|q'|}_{\ell'}(\cos\theta_{bR}) \frac{(\ell'-|q'|)!}{(\ell'+|q'|)!}\right\} \qquad (39)$$

We have separated the partial waves which reach the detector into azimuthal, polar, and radial components so that we may recognize the

factor in braces as $F^{00}_{p'q'}$, defined above. Summing over all of the (ℓ,q) partial waves gives the complete double scattered wave at the detector as

$$\psi_{ab}(\vec{R}) = \frac{e^{ika}}{a}\frac{e^{ikb}}{b}\frac{e^{ik|\vec{R}-\vec{a}-\vec{b}|}}{ik|\vec{R}-\vec{a}-\vec{b}|}\sum_{q=-1}^{1} N_{1q} R^{1}_{q0}(0,\theta_{\varepsilon a},\pi-\phi_{x\varepsilon a})\sum_{p=0}^{1-|q|} C^{1}_{pq}$$

$$\sum_{q'=-\tau}^{\tau}\sum_{p'=0}^{\tau-|q'|} e^{iq'\phi_{abR}}\, F^{00}_{p'q'}(k\vec{b},\hat{R}) \qquad (40)$$

$$*\{\frac{1}{ik}\sum_{\ell=|q'|} T_{\ell,\vec{a}}(k)\, H^{pq}_{\ell}(ka)\, 4\pi\, N_{\ell q} N_{\ell q'}\, R^{\ell}_{q'q}(0,\theta_{ab},\pi-\phi_{\varepsilon ab})\, C^{\ell}_{p'q'}\}$$

We have reordered the sums on ℓ, p', and q' to isolate the factor in braces. In that process we introduced the Taylor series order, τ, as the limit for the sums on q' and p'. The factor in braces gives the amplitude for waves of order pq to scatter off the potential at $\vec{a}$ and give waves of order p'q' in the direction of $\vec{b}$. Our next step is to define most of the factor in braces as a Taylor series spherical wave scattering factor, $F^{p'q'}_{pq}$, where F^{00}_{pq} defined above is a special case.

To this end we break up the rotation matrix into polar and azimuthal parts as given by Messiah[19]:

$$R^{\ell}_{q'q}(\alpha\beta\gamma) = e^{-i\alpha q'}\, r^{(\ell)}_{q'q}(\beta)\, e^{-i\gamma q} \qquad (41)$$

For our Euler angles we get

$$R^{\ell}_{q'q}(0,\theta_{ab},\pi-\phi_{\varepsilon ab}) = (-1)^{q}\, e^{iq\phi_{\varepsilon ab}}\, r^{(\ell)}_{q'q}(\theta_{\varepsilon a}) \qquad (42)$$

Edmonds[24] gives a formula for $r^{\ell}_{q'q}(-\theta_{\varepsilon a})$: his rotation is the inverse of Messiah's. A symmetry in the rotation matrix allows his formula to be used by switching indices:

$$r^{(\ell)}_{q'q}(\theta_{\varepsilon a}) = \left[\frac{(\ell+q)!\ (\ell-q)!}{(\ell+q')!(\ell-q')!}\right]^{1/2}$$

$$\cos^{q+q'}\left(\frac{\theta_{\varepsilon a}}{2}\right) \sin^{q-q'}\left(\frac{\theta_{\varepsilon a}}{2}\right) P^{(q-q',q+q')}_{\ell-q}(\cos\theta_{\varepsilon a}) \tag{43}$$

where $P^{(\alpha,\beta)}_{\ell}(\cos\theta)$ is the Jacobi polynomial. If $q' > q$ we use:[19]

$$r^{(\ell)}_{q'q}(\theta_{\varepsilon a}) = (-1)^{q-q'}\ r^{(\ell)}_{qq'}(\theta_{\varepsilon a}) \tag{44}$$

to avoid negative quantum numbers in the Jacobi polynomial; similarly if $q + q' < 0$ we use

$$r^{(\ell)}_{q'q}(\theta_{\varepsilon a}) = (-1)^{q-q'}\ r^{(\ell)}_{-q-q'}(\theta_{\varepsilon a}) \tag{45}$$

for the same purpose.

Removing the azimuthal dependence from the factor in braces in equation (40) leads to our scattering factor,

$$F^{p'q'}_{pq}(k\vec{a},\hat{b}) = \frac{1}{ik} \sum_{\ell=|q|_>} (2\ell+1) T_{\ell,\vec{a}}(k) H^{pq}_{\ell}(ka)\ \frac{(\ell-|q|_>)!}{(\ell+|q|_<)!}\ C^{\ell}_{p'q'}$$

$$(\cos\frac{\theta_{ab}}{2})^{|q+q'|}(\sin\frac{\theta_{ab}}{2})^{|q-q'|}P_{\ell-|q|}^{(|q-q'|,|q+q'|)}(\cos\theta_{ab}) \qquad (46)$$

We have inserted the value of $N_{\ell q}\, N_{\ell q'}$ and mean for $|q|_>$ ($|q|_<$) to be the greater (lesser) of $|q|$ and $|q'|$. We may similarly define the overlap of the direct wave with angular momenta eigenfunctions in the direction of $\hat{a}$ by

$$P_{10}^{pq}(\hat{a},\hat{\varepsilon}) = N_{1q}R^{1}_{|q|0}(0,\theta_{\varepsilon a},\pi-\phi_{x\varepsilon a})C^{1}_{pq} \qquad (47)$$

We also incorporate the signs from $N_{\ell q}$, $N_{\ell q'}$, the factor of $\exp(iq\pi)$, and the symmetry relations for the rotation matrices into:

$$S_q^{q'}=(-1)^q\ i^{|q-q'|+|q|-|q'|} \qquad (48)$$

as shown in Appendix B.

The single-scattered wave at the detector then becomes

$$\psi_a(R) = \frac{e^{ika}}{a}\frac{e^{ik|\vec{R}-\vec{a}|}}{ikR}$$

$$\sum_{q=-1}^{1}\ \sum_{p=0}^{1-|q|} F_{pq}^{00}(k\vec{a},\hat{R})\, e^{iq\phi_{\varepsilon aR}}\, P_{10}^{pq}(\hat{a},\hat{\varepsilon}) \qquad (49)$$

The double-scattered wave is:

$$\psi_{ab}(R) = \frac{e^{ika}}{a}\frac{e^{ikb}}{b}\frac{e^{ik|\vec{R}-\vec{a}-\vec{b}|}}{ikR}\sum_{q'=-\tau}^{\tau}\sum_{p'=0}^{\tau-|q|}F^{00}_{p'q'}(k\vec{b},\hat{R})S^{0}_{q'}e^{iq'\phi_{abR}}$$

$$\sum_{q=-1}^{1}\sum_{p=0}^{1-|q|}F^{p'q'}_{pq}(k\vec{a},\hat{b})S^{q'}_{q}e^{iq\phi_{\epsilon ab}}P^{pq}_{10}(\hat{a},\hat{\epsilon}) \qquad (50)$$

and the triple-scattered wave may be written by inspection. These expressions constitute our fifth small atom approximation for the multiple scattering of photoelectrons.

V. THE TAYLOR SERIES SCATTERING FACTORS

Convergence of the approximate curved-wave scattering formulae derived in the previous section requires the scattering factors $F_{pq}^{p'q'}(k\vec{a},b)$ to decrease rapidly as the Taylor indices p,q,p',q' increase. We devote this section to a discussion of these factors.

The success of plane-wave scattering models does not follow from simple convergence arguments, leading us to suspect any purely formal criteria for the Taylor series approach. Rather than pursue a general account of the convergence we will discuss some of the properties of the scattering factors using Ni atom scattering as an illustrative example.

The scattering factor depends on the four indices p,q,p', and q', on the wavenumber-distance product ka, on the scattering angle between $\hat{a}$ and $\hat{b}$, θ_{ab}, and on the potential through the scattering phase shifts $T_{\ell,a}(k)$. We refer to the superscript indices as outgoing wave indices and to the subscript indices as incoming wave indices. The single zero-order scattering factor, F_{00}^{00}, has been discussed in reference 4 (see Appendix A.); its dependence on angle and energy is qualitatively similar to the plane-wave scattering factor. As we consider larger values of the indices we find that scattering factors with non-zero outgoing wave superscripts are large while scattering factors with non-zero incoming wave subscripts are correspondingly small. When the scattered waves are formed by combining these scattering factors, large outgoing wave indices are always paired with identical incoming wave indices as the single prime indices in $F_{p''q''}^{p'q'}(kb,\hat{c})\ F_{p'q'}^{pq}(ka,\hat{b})$, but this behavior makes convergence difficult to discuss. Thus we will rescale

the scattering factors so that they may stand alone. Our development of this rescaled factor will also serve as our introduction to the nature of the scattering factors.

Our goal for the rescaled scattering factor is to isolate the dominate character of $F_{pq}^{p'q'}$ which allows it to converge as p and q increase and to split this character between the incoming and outgoing waves. The incoming wave indices p and q appear in the integral $H_{\ell}^{pq}(ka)$; the q index also appears in the angle functions, which we discuss first.

The angle dependent terms in the scattering factor are:

$$A_{qq'}(\theta_{ab}) =$$

$$[\cos \frac{\theta_{ab}}{2}]^{|q+q'|} [\sin \frac{\theta_{ab}}{2}]^{|q-q'|} P_{\ell-|q|_>}^{(|q-q'|,|q+q'|)}(\cos \theta_{ab}) . \qquad (51)$$

For the purpose of rescaling the scattering factor we may ignore these angle terms: their product always has a magnitude less than, but on the same scale as 1.0. In passing, we note that the angle dependence requires that

i) only factors with q=q' contribute to forward (θ_{ab}=0) scattering,

ii) only factors with q=-q' contribute to backscattering (θ_{ab}=π),

iii) the angular factors do not change if both q and q' are simultaneously negated or if q and q' are switched,

iv) the angular factors alternate sign with increasing ℓ for $\theta>\pi/2$.

Item iii) is a consequence of the symmetry relations of the rotation matrix elements and, coupled with the observation that all the remaining dependence on q and q' in the scattering factor uses only their magnitudes, we have this important relation:

$$F_{pq}^{p'q'}(k\vec{a},\hat{b})=F_{p-q}^{p'-q'}(k\vec{a},\hat{b}). \tag{52}$$

With no strong dependence on q in the angular factors, we must turn to $H_\ell^{pq}(ka)$ for our rescaling relation. If we use the explicit formula from appendix C, ref. 13, we may write:

$$F_{pq}^{p'q'}(k\vec{a},\hat{b})= \frac{1}{ik}\frac{(-1)^p}{(ika)^{p+q}}\frac{p!}{q!}\sum_{s=0}^{p}\frac{(p+q-s)!}{s!(p-s)!}(ka)^s\sum_{\ell=|q|_>}(2\ell+1)T_{\ell,\vec{a}}(k)\frac{\partial^s d_\ell(ka)}{\partial(ka)^s}$$

$$\frac{(\ell+|q|)!}{(\ell-|q|)!}\frac{(\ell-|q|_>)!}{(\ell+|q|_<)!}\frac{(\ell+|q'|+p')!}{(\ell-|q'|-p')!}\frac{1}{p'!\ (2|q|+2p)!!}A_{qq'}(\theta_{ab}) \tag{53}$$

The leading term and the factorial terms containing ℓ in this equation reiterate an earlier theme from our discussion of the convergence of the small atom approximations in section III: the size of these scattering factors is determined by $\ell(\ell+1)/ka$. The product of factorials depending on ℓ in this form of the scattering factor may be expanded into a

polynomial in ℓ^2 whose highest power is $p'+(|q'|+|q|)/2$. From these results we propose a rescaled scattering factor according to

$$\bar{F}^{p'q'}_{pq}(k\vec{a},\hat{b}) = \frac{(kr_0)^{p+|q|/2}}{(kr_0)^{p'+|q'|/2}} F^{p'q'}_{pq}(k\vec{a},\hat{b}) \qquad (54)$$

Empirically we find that all the rescaled factors for nearest neighbor scattering are of a similar size. (We must also apply this rescaling to the photoemission factors, $P^{p'q'}_{10}$, to insure that the scaling always cancels when the wavefunctions are constructed.)

If we estimate the scattering radius by $|f(\theta,k)|/2$, our rescaled scattering factor is roughly proportional as

$$\bar{F}^{p'q'}_{pq}(k\vec{a},\hat{b}) \sim \alpha \left(\frac{r_0}{a}\right)^{p+q} \left(\frac{|f(\theta,k)|}{2r_0}\right)^{p'+(q'+q)/2} \left(\frac{k|f(\theta,k)|}{2}\right)^{p'+(q'+q)/2} \qquad (55)$$

The first term in this expression contains increasing powers of (r_0/a), the angle subtended by the radius of the potential at a distance $|\vec{a}|$ from the wave source. Thus if we compare scattering factors at a bond length of $|\vec{a}|$ and $2|\vec{a}|$, we will find that first order terms are half as large, the second order terms are one-fourth as large and so on. The second term may be interpreted as correcting the scattering potential radius to account for the scattering angle differences: forward scattering angles will have $[|f(\theta,k)|/2]\approx r_0$ while backscattering only uses the central region of the potential, $[|f(\theta,k)|/2]<<r_0$. Hence the

convergence in backscattering is much more rapid. Finally, the last term reminds us that the convergence does not improve with energy; it may indeed worsen.

Representative examples of second order scattering factors for nearest neighbor Ni atom scattering are illustrated in figures 4, 5, and 6. The more rapid convergence in backscattering is evident by the small values of the higher order scattering factors for angles $>90^{\circ}$, and a first order Taylor series appears adequate for backscattering. Forward angles may require higher than second order.

VI. DISCUSSION

In the previous section we have shown that Taylor series terms of order τ fall off as $(1/ka)^{\tau}$ where a is the bond length between scattering atoms, and we suggested that the size of the Taylor terms is governed by $(r_o/a)^{\tau}$.

In this section we will

i) discuss the zero order term which survives at larger bond lengths,

ii) give an example of the convergence of the series for a particular nearest neighbor scattering,

iii) describe the magnetic quantum number expansion view of the physical nature of the Taylor series small atom approximation, and

iv) describe how this alternative view predicts rapid convergence of the Taylor expansion for multiple scattering ARPEFS problems.

We begin with the zero-order Taylor series term. With $\tau = 0$, the scattering equations from section IV contain only one scattering factor for each event:

$$F_{00}^{00}(\hat{ka},\hat{b}) = \frac{1}{ik}\sum_{\ell=0}(2\ell+1)T_{\ell}(k)d_{\ell}(ka)P_{\ell}(\cos\theta_{ab}). \qquad (56)$$

This is exactly equal to the homogeneous wave scattering factor f_{ab}^{00}: the homogeneous wave model introduced in section III is the zero-order Taylor series term. This means that the zero-order term represents the scattering of spherical Hankel functions at their asymptotic limit, but

it contains the 1/kr variation of $h_0(kr)$ radially along the potential. Note that the zero-order term is not the plane-wave model, but, as discussed in ref 4, the difference between the plane-wave factor f_{ab}^{plane} and f_{ab}^{00} is small for backscattering angles. Coupled with rapid convergence of the Taylor series for backscattering angles, we conclude that the plane-wave approximation may be adequate for many backscattering problems.

The same may not be said for scattering angles closer to zero. To give some feel for the size of the corrections for forward scattering, we have calculated the ARPEFS oscillations for a particularly important geometry. We have selected our problem from the experimental study of ref 1: we consider S(1s) photoabsorption from c(2x2)S/Ni(100) with both the emission and polarization vectors along the [110] crystallographic direction. We concentrate on only two scattering events, single scattering from the Ni atom directly behind the S photoemitter and forward scattering of this backscattered wave through the S emitter. The path-length difference between these scattered waves and the direct wave are nearly equal at ~ 4.4Å, corresponding to the dominant frequency in the experimental measurements. The backscattering angle is 173° while the forward angle is 7°.

The results of these calculations are displayed in Figures 7 and 8 as

$$\chi(k) = \frac{\psi_s^* \psi_s - \psi_o^* \psi_o}{\psi_o^* \psi_o} \qquad (57)$$

where

$$\psi_s = \psi_o + \psi_a + \psi_{ab} \tag{58}$$

for $\vec{a}$ running from the S emitter to the Ni scattering atom and $\vec{b} = -\vec{a}$. Figure 7 compares plane-wave calculations with the "exact" spherical wave calculation based on the Gaunt integral summation. The oscillations in the plane wave case are much larger even though the plane wave model slightly underestimates the forward scattering amplitude. This means that the most of the discrepancy is the phase error made in the plane-wave forward scattering. The forward scattering phase shift estimated by the plane-wave model is too small. Thus the single scattered and double scattered waves are nearly in phase and their sum has an amplitude 170% of the single scattering amplitude. With the correct forward-scattering phase-shift, the double-scattered wave is ~ $\pi/2$ out of phase with the single scattered wave and the sum has a more modest amplitude.

Figure 8 illustrates the Taylor series model results. We are able to display only the zero-order result on this scale: the first-order Taylor series cannot be distinguished from the exact calculation. Thus at least for this important scattering geometry, the Taylor series is converged at first order. Our alternative view of the Taylor model which we develop next will help to understand this remarkable convergence and will lead into our discussion of more general scattering geometries.

Before leaving figure 8 we note that the phase of the zero order (homogeneous wave) result is accurate while the amplitude is too large. This means that important differences between the asymptotic limit of

the spherical Hankel functions and the plane-wave limit appear in the phase of the double scattered wave. We have also calculated (but not plotted) these scattering events with the hybrid renormalized homogeneous wave model described in section III: we find a curve roughly half way between the zero and first order results.

The surprising success of the first order Taylor expansion has an interesting origin which will lead to the third topic of this section, the MQNE description of the Taylor expansion. The first-order Taylor expansion is accurate because the origin-shift addition theorem does not change the magnetic quantum number if the shift is parallel to the z axis[13]. For the scattering geometry we selected, the outgoing photoemission wave has $m = 0$ along the electric vector. Since the scattering atom vector is nearly parallel to $\vec{\epsilon}$, the scattered partial waves will also have $m = 0$, even if they now have ℓ from 0 to ℓ_{max}. Encountering the sulfur atom and scattering into the detector will give double scattered partial waves also with $m = 0$ along $\vec{\epsilon}$. Thus to a fair approximation we need only $m = 0$ waves for the entire problem.

What of a more general geometry? Consider, for example, scattering first from the Ni atom directly behind the sulfur atom followed by scattering from another nearest neighbor Ni atom. Then the second scattering vector, $\vec{b}$, will no longer lie parallel to $\vec{a}$. To use the result that m will not change for z axis shifts we must rotate the $m = 0$ partial waves emanating from the Ni atom at $\vec{a}$ to the $z||b$ system. This rotation will include all magnetic sublevels $-\ell \leq m' \leq \ell$ in the $z||b$ system in proportion to the overlap integral (rotation matrix element) between

spherical harmonics in the two systems. These manifold sublevels are not, however, equally effective in scattering from the second Ni atom. As illustrated in Fig. 9, the m=0 spherical harmonics overlap the potential along the scattering bond length, m = 1 waves overlap the potential farther from the axis and so on until some m = τ sublevel does not overlap the potential at all. Thus only the τ lowest magnetic sublevels need be overlapped with the m = 0 waves and--by Nozawa's result--only the τ lowest sublevels will appear on center b as scattered waves. For a triple scattering event, these lowest τ sublevels will need to be rotated to τ sublevels along the new scattering axis. Hence we identify the rotated-frame magnetic sublevels with the q index in the Taylor expansion model.

We can push this picture farther by comparing the classical orbits sketched in Fig. 3 to the incident spherical harmonics in Fig. 9. The largest magnetic sublevels only overlap the outer regions of the potential, regions which contribute to forward scattering, not backscattering. This would suggest, again, that the Taylor series will converge much more quickly for backscattering.

VII. CONCLUSION

We have explored five small atom approximations. Some specific points bear summarizing here:

i) the success of plane wave models relies on backscattering geometries,

ii) the plane-wave model requires incident waves at their asymptotic limit and a small diameter potential; it is inappropriate for multiple scattering calculations in solids,

iii) the point-scattering and homogeneous-wave models are inadequate for multiple scattering in the intermediate energy range, at least for near neighbor scattering,

iv) the homogeneous-wave model is the zero-order Taylor series term,

v) the Taylor series model allows methodical improvement in scattering calculations, and it follows from physically appealing magnetic quantum number expansion picture of the scattering partial waves.

We have also developed the multiple scattering equations for ARPEFS with the Taylor series expansion of the origin-shift addition theorem and illustrated the results with a two atom model.

The most direct extension of this work would be the application of the Taylor expansion method to simulations of experimentally measured ARPEFS curves. In addition to the elastic, multiple scattering equations derived here, we must also include important inelastic scattering factors and effects such as finite aperture integration before quantitative agreement with experiment could be expected.

Under the appropriate development, the MQNE origin-shift addition theorem will also give multiple scattering models for other spectroscopies based on electron scattering in the intermediate energy range. EXAFS should yield to a low order expansion since the multiple

scattered wave must always return to the absorbing atom: forward scattering will necessarily be coupled with backscattering as in the example in section VI. Electron diffraction in the 100-600 eV range should also be amenable to the treatment given here with the direct wave replaced by the incident plane wave. The first scattered wave will, of course, then be given exactly by the plane wave scattering factor.

The Taylor series expansion itself deserves further exploration. Accurate error bounds would eliminate empirical verification of convergence. Alternate parameterization of the scattering factors might reduce the computation burden required for the scattering calculations. The magnetic quantum number expansion picture suggests that a variation of the equations presented here could be built up from rotation matrices and Nozawa's origin-shift formulas. Finally, the formulation of the exact multiple scattering equations (matrix inversion method) with the Taylor series result should be examined. At least pairwise or colinear multiple scattering seems feasible but more complex geometries would require detailed study.

APPENDIX A. COMPARING NOTATION WITH REF. 4

We have deduced a formula equivalent to eqn. (37) for the exact curved wave scattering of $\ell=1$ waves in ref. 4; we demonstrate that equivalence here. The single-scattered wave from ref. 4 may be written

$$\psi_{\vec{a}}(\vec{R}) = \left(\frac{3}{4\pi}\right)^{1/2} \frac{e^{ik|\vec{R}-\vec{a}|}}{ikR} \frac{e^{ika}}{a} \{d_1(ka)\cos\theta_{\varepsilon a} f_{aR}^{00}$$

$$-i\cos\theta_{\varepsilon a} f_{aR}^{10} - \frac{i}{ka}\sin\theta_{\varepsilon a}\sin\theta_{aR}\cos\phi_{\varepsilon aR} f_{aR}^{01}$$

where

$$f_{aR}^{nm} = \frac{1}{ik}\sum_{\ell=0}(2\ell+1)T_\ell(k)\frac{\partial^n d_\ell(ka)}{(\partial ka)^n}\frac{\partial^n P_\ell(\cos\theta_{aR})}{\partial(\cos\theta_{aR})}.$$

From our new definition we have

$$\cos\theta_{\varepsilon a} F_{00}^{00} + \cos\theta_{\varepsilon a} F_{10}^{00} = \frac{\cos\theta_{\varepsilon a}}{ik}\sum_{\ell=0}(2\ell+1)T_\ell(k)P_\ell(\cos\theta)[H_\ell^{00}+H_\ell^{10}]$$

and from Appendix C, ref. 13

$$H_\ell^{00} + H_\ell^{10} = \left[\frac{\ell+1}{2\ell+1}\right] d_{\ell+1} + \frac{\ell}{2\ell+1} d_{\ell-1}.$$

Using eqn. B9 in Ref. 4, the right side becomes

$$H_\ell^{0\,0} + H_\ell^{10} = d_\ell - \frac{d_\ell}{ikr} - i\frac{\partial d_\ell(ka)}{\partial(ka)}$$

Working back through the definition of f_{aR}^{00} and f_{aR}^{10} shows that

$$\cos\theta_{\varepsilon a}F_{00}^{00} + \cos\theta_{\varepsilon a}F_{10}^{00} = d_1(ka)\cos\theta_{\varepsilon a}f_{aR}^{00} - i\cos\theta_{\varepsilon a}f_{aR}^{10}.$$

where $d_1(ka) = 1 + i/ka$. Similarly we write out

$$F_{01}^{00}(\vec{a},\vec{R}) = \frac{1}{ik}\sum_{\ell}(2\ell+1)T_\ell(k)\frac{P_\ell(\cos\theta)}{(2\ell+1)}[d_{\ell-1}-d_{\ell+1}]$$

where a factor of $\ell(\ell+1)$ in H_ℓ^{pq} cancels the last factorial in the definition of F_{01}^{00}. The connection between associated Legendre polynomials and derivatives of Legendre polynomials:

$$P_\ell^m(\cos\theta) = \sin^m\theta\,\frac{d^m{}_\ell(\cos\theta)}{d(\cos\theta)^m}$$

and the recursion for d_ℓ gives

$$\sin\theta_{\varepsilon a}\cos\phi_{\varepsilon aR}F_{01}^{00}(\vec{a},\vec{R}) = \frac{\sin\theta_{\varepsilon a}\cos\theta_{\varepsilon aR}\sin\theta_{aR}}{ikr}f_{aR}^{01}.$$

These close connections demonstrate that i) the differential formula of ref. 4 could be used as a basis for a Taylor expansion, ii) the rotation matrix approach employed here for approximate origin shift will lead to compact exact origin shift formulas, and iii) individual scattering factors F_{pq}^{00}, and by extension $F_{pq}^{p'q'}$, can be interpreted as specific spherical wave corrections as described in ref 4 and 13. Our new formulation is recommended for numerical work.

APPENDIX B. ON THE SIGN FACTOR $S_q^{q'}$

The sign of the Taylor series scattering factor is a combination of the signs in the definition of $N_{\ell q}$:

$(-1)^q$ $\quad q \geq 0$

(1) $\quad q < 0,$

the factor of $\exp(i\pi q)$ from the rotation matrix, and the symmetry relations for rotation matrices. Note that the symmetry relations are applied depending on the sign of $q-q'$ and $q+q'$; we have four cases:

i) $q + q' \geq 0,\ q - q' \geq 0$

$$r^{\ell}_{q'q}(\beta) = r^{\ell}_{q'q}(\beta)$$

ii) $q + q' \geq 0,\ q-q' < 0$

$$r^{\ell}_{q'q}(\beta) = (-1)^{q+q'} r^{\ell}_{qq'}(\beta)$$

iii) $q + q' < 0,\ q -q' \geq 0$

$$r^{\ell}_{q'q}(\beta) = r^{\ell}_{-q-q'}(\beta)$$

iv) $q + q' < 0,\ q - q' < 0$

$$r^{\ell}_{q'q}(\beta) = (-1)^{q-q'} r_{q'-q}(\beta)$$

In case iii) the factors of $(-1)^{q-q'}$ cancel from successive symmetry relations; in cases iii) and iv) the criterion for equation (44) to apply changes since equation (45) negates the indices. Surveying these cases shows that only when $(q-q') < 0$ will factors of (-1) be required.

To summarize these factors we note that

$|q| + q = 0$ $\quad$ if $\quad q \leq 0$

$= 2|q|$ $\quad$ if $\quad q > 0$

while

$$|q-q'| - (q-q') = 2|q-q'| \qquad \text{if } (q-q') \leq 0$$

$$= 0 \qquad \text{if } (q-q') > 0.$$

All of the factors may be written then as

$$S_q^{q'} = (-1)^q \, i^{|q-q'|-(q-q')} \, i^{|q|+q} \, i^{|q'|+q'},$$

or since $i^{4|q'|} = 1$,

$$S_q^{q'} = (-1)^q \, i^{|q-q'|+|q|-|q'|}.$$

ACKNOWLEDGEMENTS

This work was supported by the Director, Office of Energy Research, Office of Basic Energy Sciences, Chemical Sciences Division of the U.S. Department of Energy under Contract No. DE-AC03-76SF00098.

REFERENCES

1. J.J. Barton, C.C. Bahr, Z. Hussain, S.W. Robey, J.G. Tobin, L.E. Klebanoff, and D.A. Shirley, Phys. Rev. Lett. 51, 272 (1983).

2. P.A. Lee, P.H. Citrin, P. Eisenberger, and B.M. Kincaid, Rev. Mod. Phys. 53, 769 (1981).

3. B.K. Teo, J. Am. Chem. Soc. 103, 3990 (1981); J.J. Boland, S.E. Crane, and J.D. Baldeschwieler, J. Chem. Phys., 77, 142 (1982).

4. J.J. Barton and D.A. Shirley, "Curved Wavefront Corrections for Photoelectron Scattering," LBL-18692 , and submitted to Phys Rev. B

5. J.B. Pendry, Low Energy Electron Diffraction, Academic Press, London, (1974).

6. S.Y. Tong, C.H. Li, "Diffraction Effects in Angle-Resolved Photoemission Spectroscopy" in Chemistry and Physics of Solid Surfaces V.III, CRC Press, Boca Raton, Florida, 1982.

7. B.A. Bunker and E.A. Stern, Phys. Rev. B 27, 1017 (1983).

8. P.A. Lee and J. B. Pendry, Phys. Rev. B 11, 2795 (1975).

9. V.A. Biebesheimer, E.C. Marques, D.R. Sandstrom, F.W.Lytle, and R.B. Greegor, J.Chem. Phys., 81, 2599 (1984)

10. C.H. Li and S.Y. Tong, Phys. Rev. Lett. 43, 526 (1979).

11. P.J. Durham, J.B. Pendry, and C.H. Hodges, Comp. Phys. Comm. 25, 193 (1982).

12. C. Cohen-Tannoudji, B. Diu, F. Laloe, Quantum Mechanics, John Wiley and Sons, New York, 1977.

13. J.J. Barton, and D.A. Shirley, "Approximate Translation of Screened Spherical Waves," LBL-19076, and submitted to Phys Rev. A.

14. R. Nozawa, J. Math. Phys. 7, 1841 (1966).

15. P.A. Lee, Phys. Rev. B 13, 5261 (1976).

16. P.J. Orders and C.S. Fadley, Phys. Rev. B 27, 781 (1983).

17. L.I. Schiff, Quantum Mechanics, 3rd edition, McGraw-Hill, New York, 1968.

18. J.A. Gaunt, Phil. Trans. Roy. Soc. (London) A228, 151, (1924).

19. A. Messiah, Quantum Mechanics, John Wiley and Sons, New York (1958).

20. M. Abramowitz and I.A. Stegun, Handbook of Mathematical Functions, National Bureau of Standards, Appl. Math. Services 55, (1964).

21. L. McDonnell, D.P. Woodruff, and B.W. Holland, Surf. Sci. 51, 249 (1975).

22. H. Daimon, H. Ito, S. Shin, and Y. Murata, J. Phys. Soc. Japan, 53, 3488 (1984).

23. A.R. Edmonds, Angular Momentum in Quantum Mechanics, 2nd ed. Princeton University Press, Princeton, NJ (1960).

24. B.A. Bunker and E.A. Stern, Phys Rev. B, 27, 1017 (1983).

Figure Captions

Figure 1. Definition of the vectors used in our scattering equations. The electric vector is represented by $\hat{\epsilon}$. We place the origin at the photo-emitter, the detector lies along $\vec{R}$. Vectors $\vec{a}$, $\vec{b}$, and so on run from one scattering atom to the next.

Figure 2. Schematic illustration of four small-atom approximations described in Section III, plotted along the scattering vector $\vec{a}$. Every panel contains, as the dotted curve, a graph of the imaginary part of the spherical Hankel function for $\ell = 7$, $k = 8\text{Å}^{-1}$. The abscissa gives the distance from the wave function origin in Å. Each panel also contains an arrow centered at 2.23Å, the S-Ni bond length for c(2x2)S/Ni(100), to indicate the extent of a Ni atom potential of effective radius 0.8Å. (a) Plane-wave model, functional dependence agrees with spherical wave but has errors in phase and amplitude. (b) Point-scattering model, phase and amplitude correct at $r = 2.23$Å, errors in both at the edges of the Ni potential. (c) Homogeneous-wave model, correct in (1/kr) dependence of amplitude, errors in phase, some small errors in amplitude at edge of Ni potential. (d) Hybrid, renormalized homogeneous-wave method, substantially correct over the range of the potential, some error at the small r edge of the Ni atom.

Figure 3. Schematic semiclassical orbits for an attractive potential. If the circle represents the effective radius of a screened nuclear charge, then particles with large impact parameters will sample only the weak outer region of the potential and scatter through small (forward) angles. Particles with small impact parameters orbit the strong nuclear attraction and exit at large (backscattering) angles. The connection to wave scattering is made through $b = \ell/k$ where b is the impact parameter: large ℓ partial waves contribute to forward scattering and small ℓ waves dominate for backscattering.

Figure 4. Taylor series scattering factor amplitude at $k = 8\text{Å}^{-1}$, $|\vec{a}| = 2.23\text{Å}$, as a function of scattering angle, θ_{ab}. The scattering factors generally have similar shapes whenever they agree in $|q-q'|$ and $|q+q'|$; hence we will only plot representative examples. We adopt the notation $(p'q'|pq)$. (a) solid line $(00|00)$, an example of factors with $|q-q'| = 0$, $|q+q'| = 0$. This is the single zero order factor. (b) circles $(01|10)$, $|q+q'| = 1$, $|q-q'| = 1$. (c) crosses $(02|20)$, $|q+q'| = 2$, $|q-q'| = 2$. Factors are multiplied by 3 after the break at 60°; the right hand scale applies to this region.

Figure 5. Same as figure 4; note the increased scales. (a) solid line $(00|01)$, $|q-q'| = 1$, $|q+q'| = 1$; (b) circles $(01|01)$, $|q-q'|$

= 0, $|q+q'| = 2$ (c) crosses (02/01), $|q-q'| = 1$ $|q+q'| = 3$; (d) plus symbols (02/02), $|q-q'| = 0$, $|q+q'| = 4$.

Figure 6. Same as figure 4. (a) solid line (11/20) $|q-q'| = 1$, $|q+q'| = 1$. (b) circles (01/1-1), $|q-q'| = 2$, $|q+q'| = 0$. (c) crosses (02/1-1), $|q-q'| = 3$, $|q+q'| = 1$. (d) plus symbols (02/0-2), $|q-q'| = 4$, $|q+q'| = 0$.

Figure 7. ARPEFS oscillations calculated by exact Gaunt integral summation (thick curve) and plane wave approximation (thin curve). These curves simulate the fractional oscillation of the S (1s) partial cross-section from c(2x2)S/Ni(100) along [110], but consider only a single Ni atom scatterer. The inset diagram illustrates the three waves which sum to give the photoemission final state, the direct, single-scattered, and double-scattered waves. The backscattering angle is 173°; the forward angle is 7°. Both curves have been multiplied by $\exp(-0.02k^2-2.23/.173k)$ (Debye Waller and inelastic attenuation) to give a more realistic amplitude comparison.

Figure 8. Same as figure 7 except comparing the exact Gaunt summation to the zero order Taylor series result. The first order Taylor result cannot be distinguished from exact, on this scale.

Figure 9. Schematic illustration of the magnetic quantum number expansion interpretation of eqn. (31). A polar plot of the four lowest magnetic sublevels of a $\ell=7$ spherical harmonic is superimposed upon a circle whose radius represents the effective radius r_0 of a nearest neighbor potential. The line connecting the incident wave source and the potential origin is used for the spherical harmonic polar axis and only the region of angles near the pole is plotted. The angle functions have been rescaled to place their first maxima on the same radius. The m=0 sublevel (solid line) is seen to overlap the strong central portion of the potential, while the m=1 lobes (dotted line) peaks further from the axis. The m=2 lobes (dot-dash lines) only intercept the far edges of the potential and the m=3 level (dashed lines) completely missed the mark.

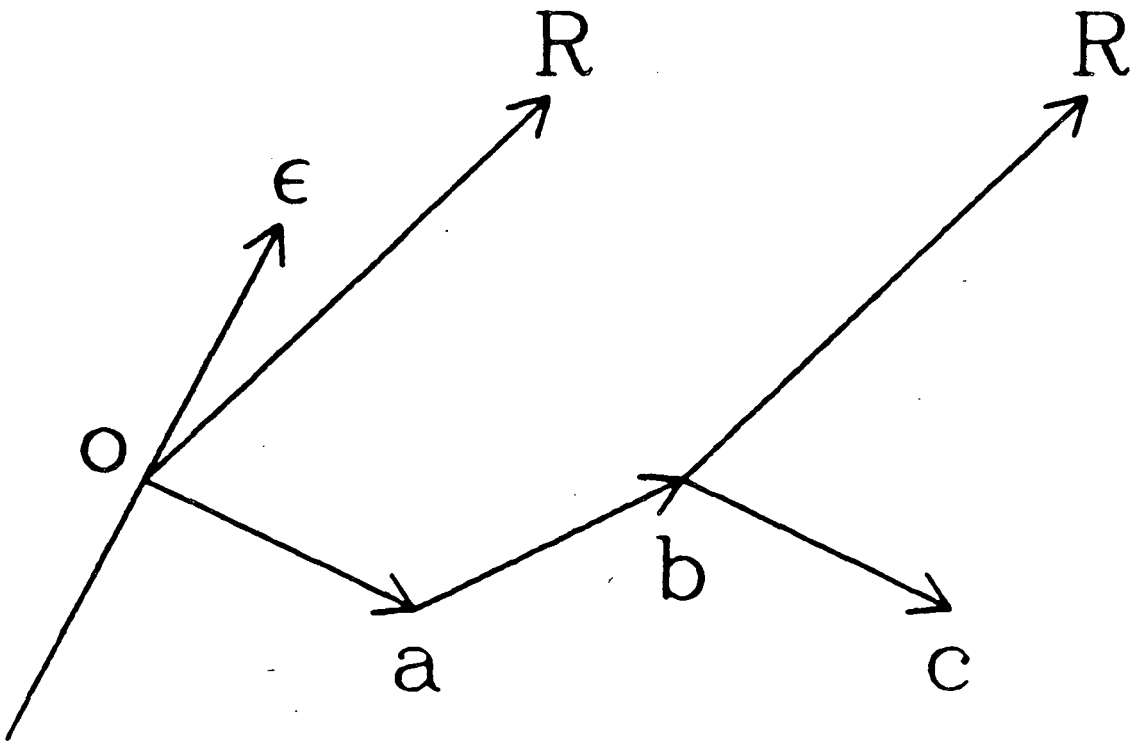

XBL 851-1020

Figure 1

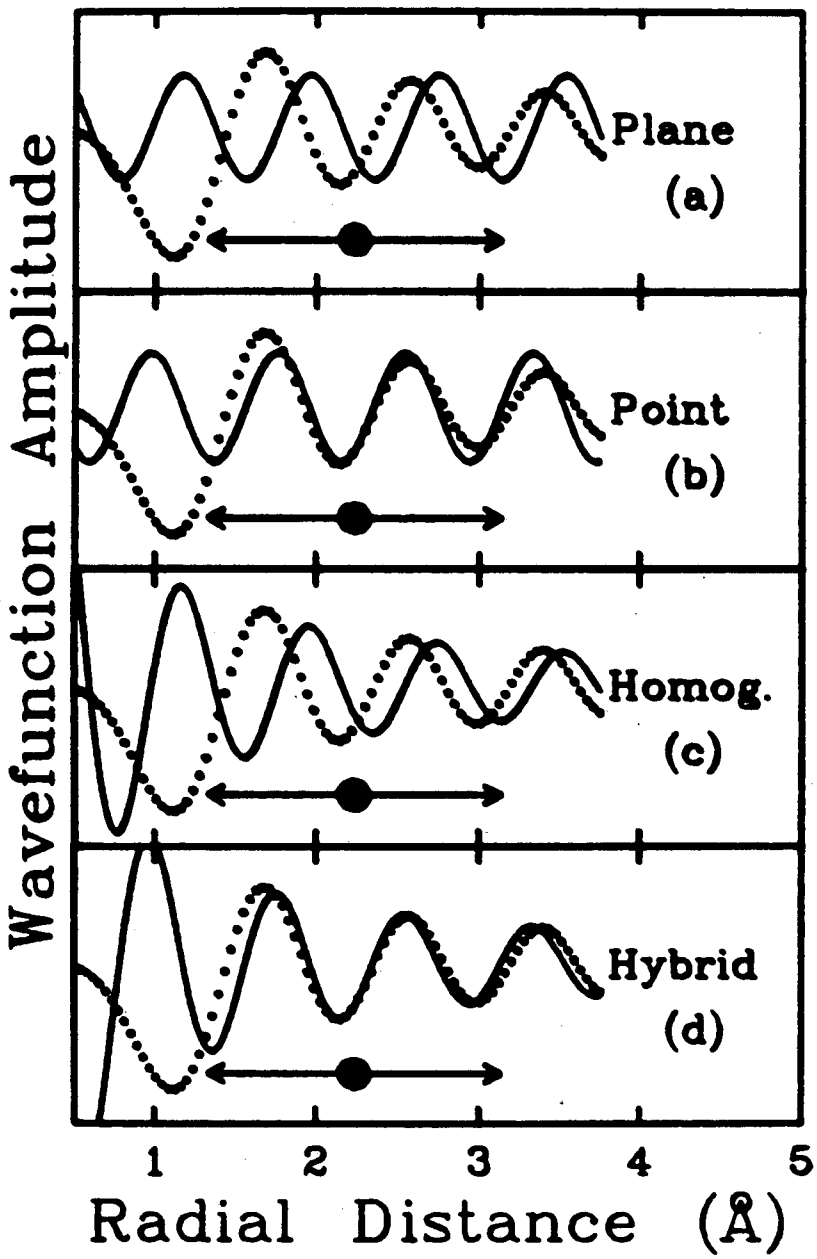

XBL 851-1022

Figure 2

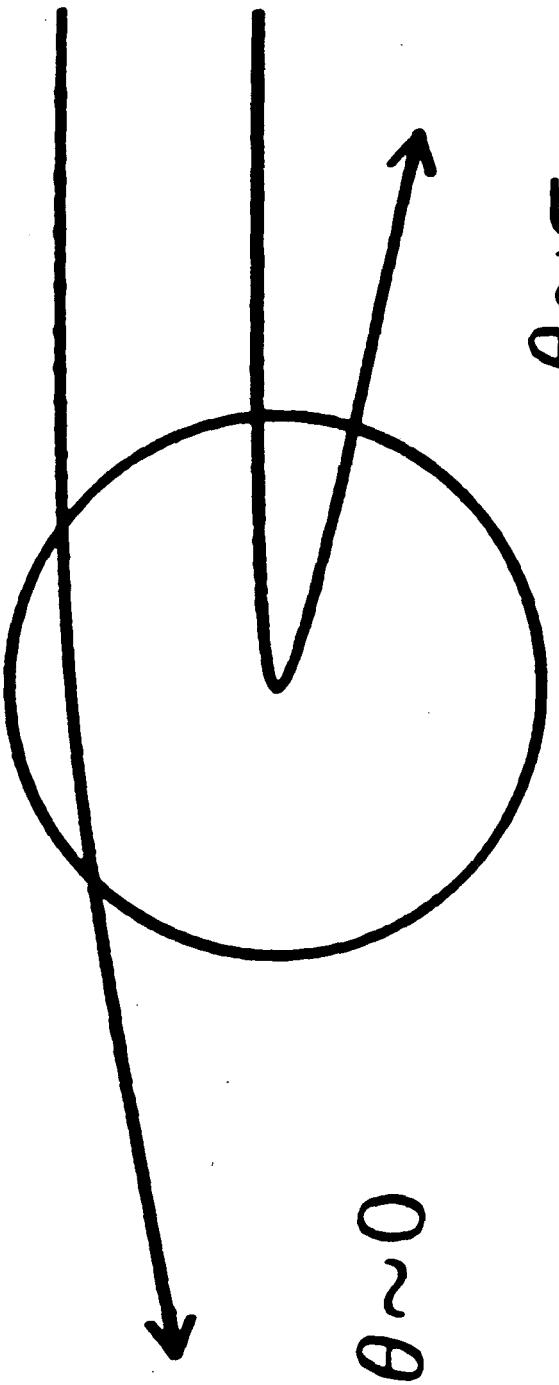

XBL 851-1021

Figure 3

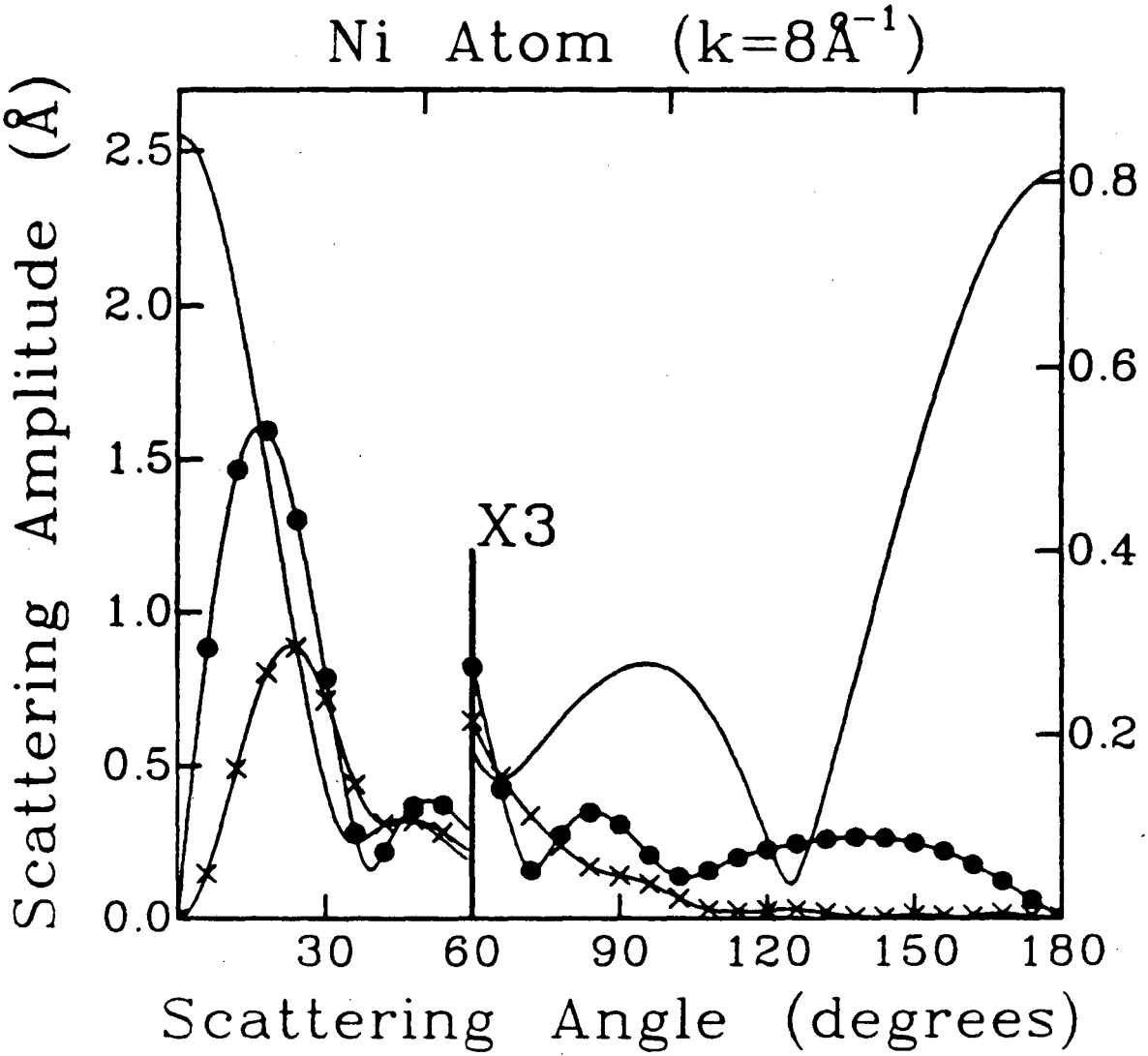

XBL 851-1017

Figure 4

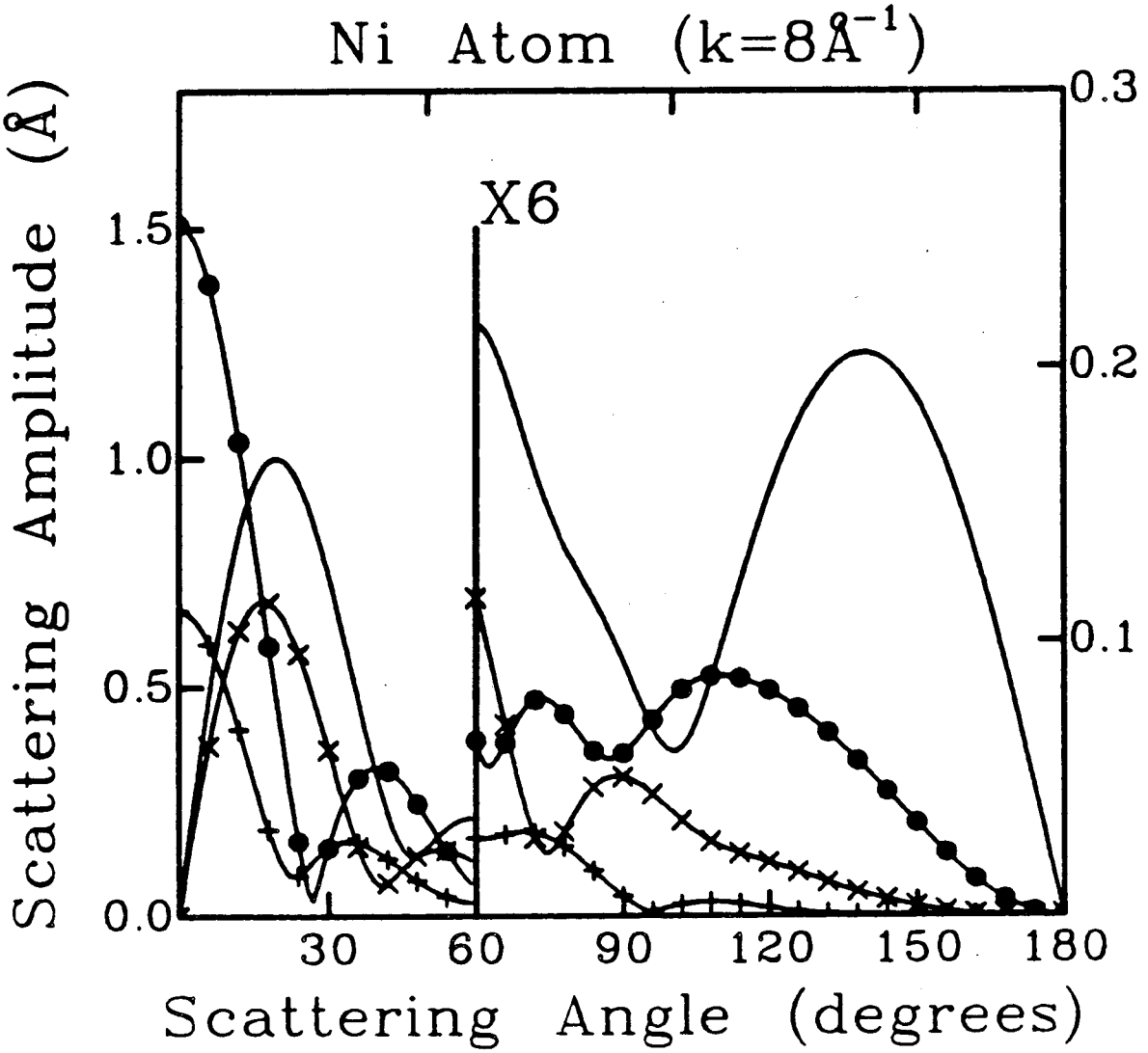

XBL 851-1016

Figure 5

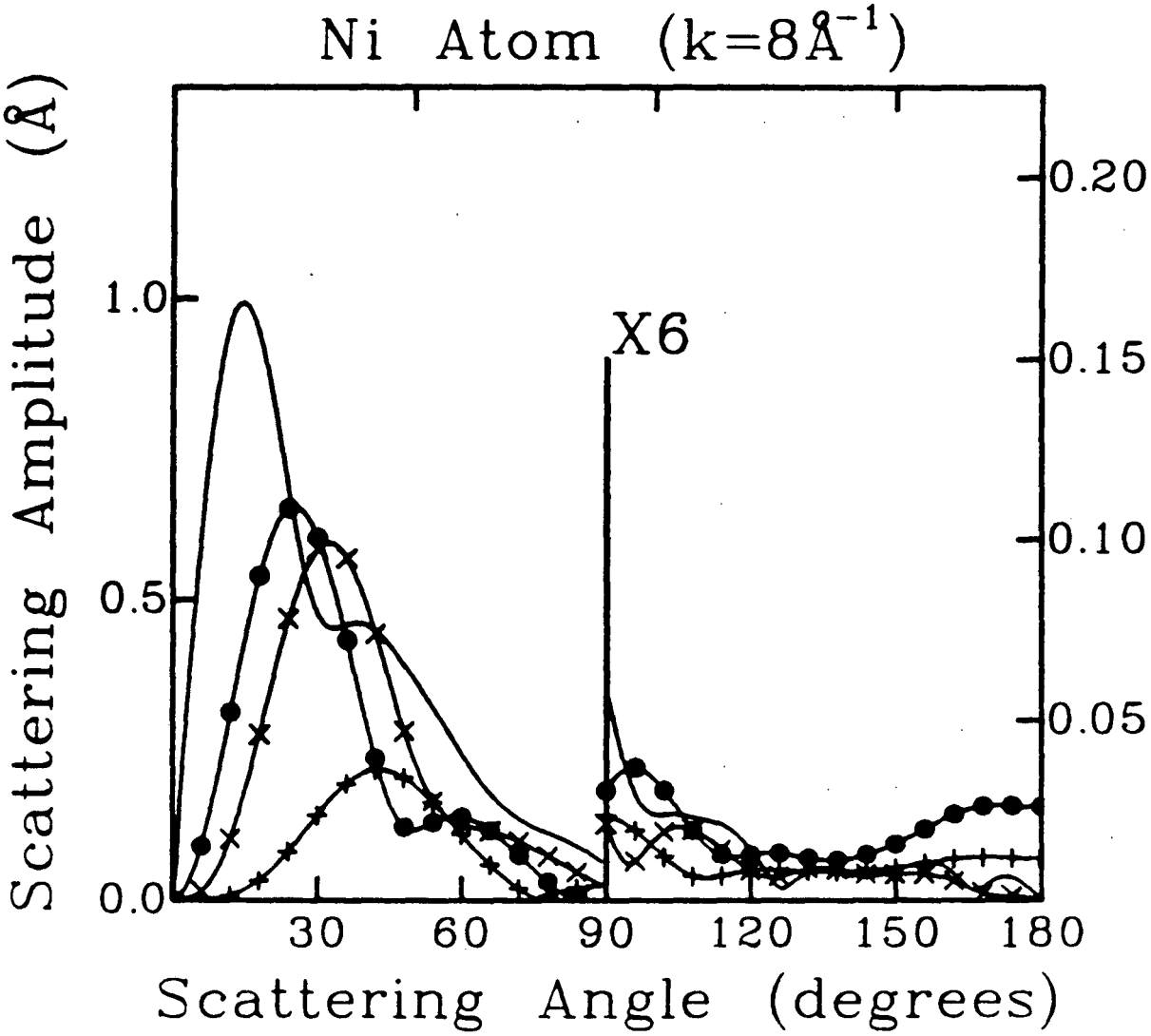

XBL 851-1018

Figure 6

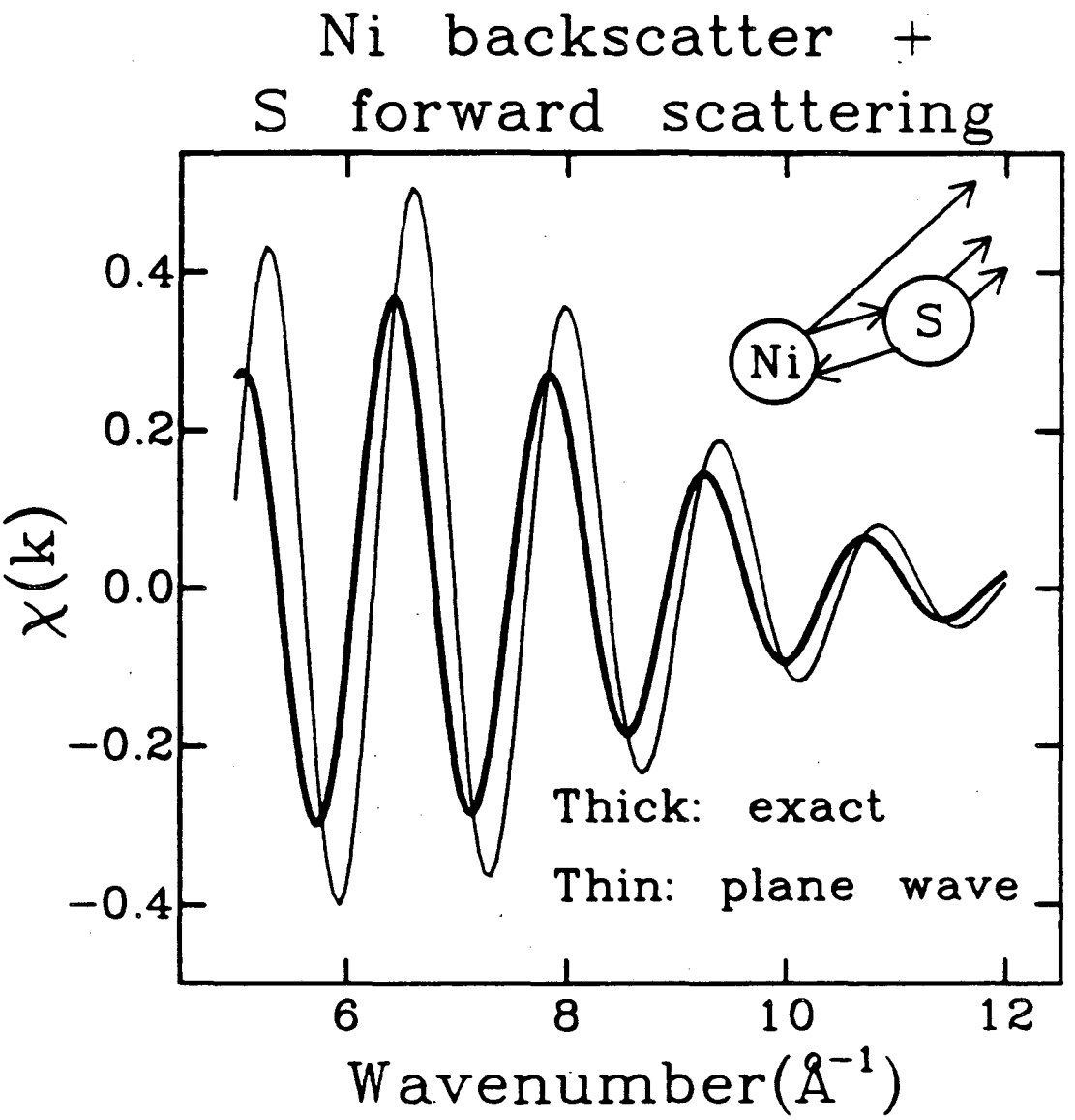

XBL 851-1023

Figure 7

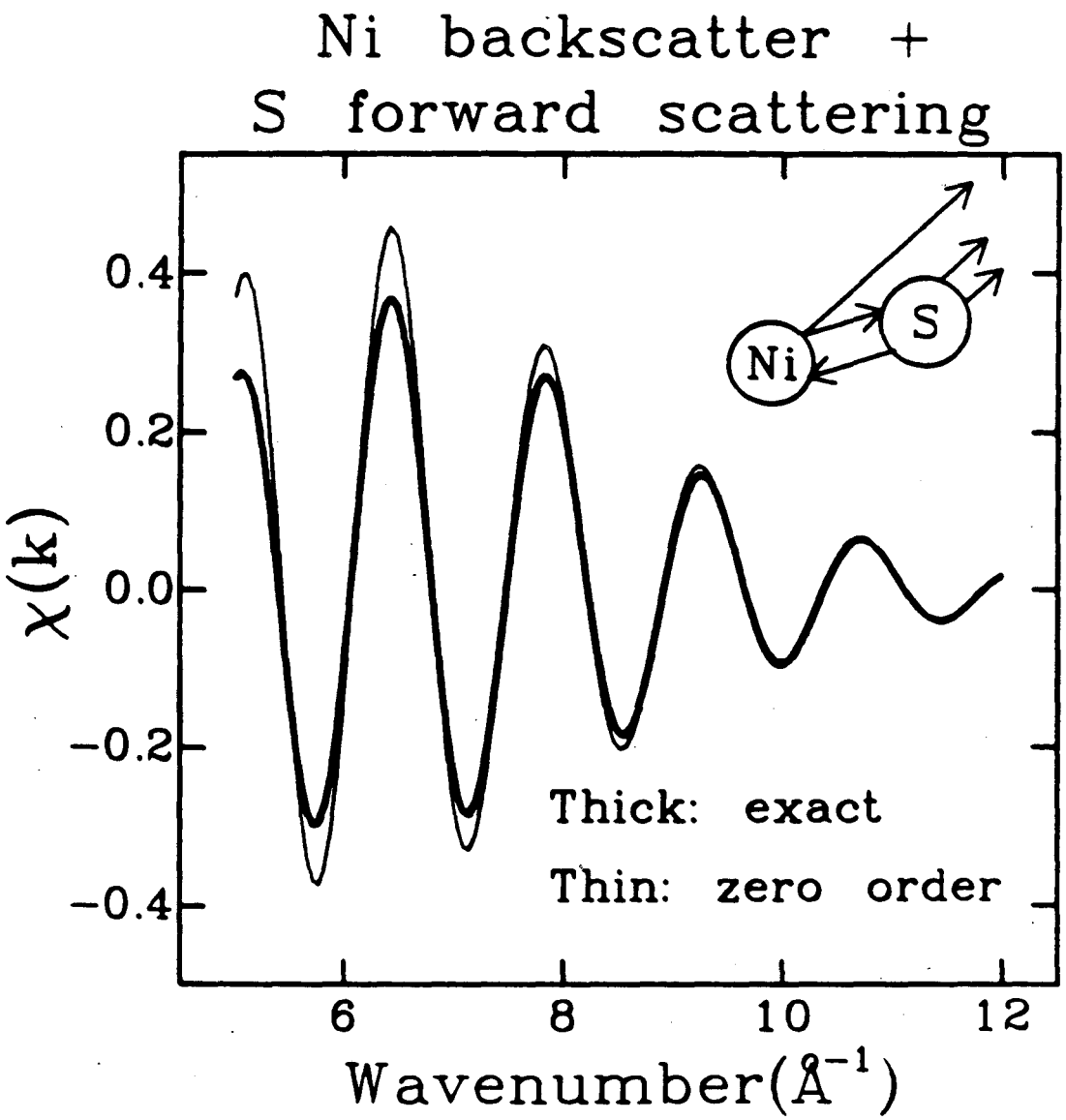

XBL 851-1024

Figure 8

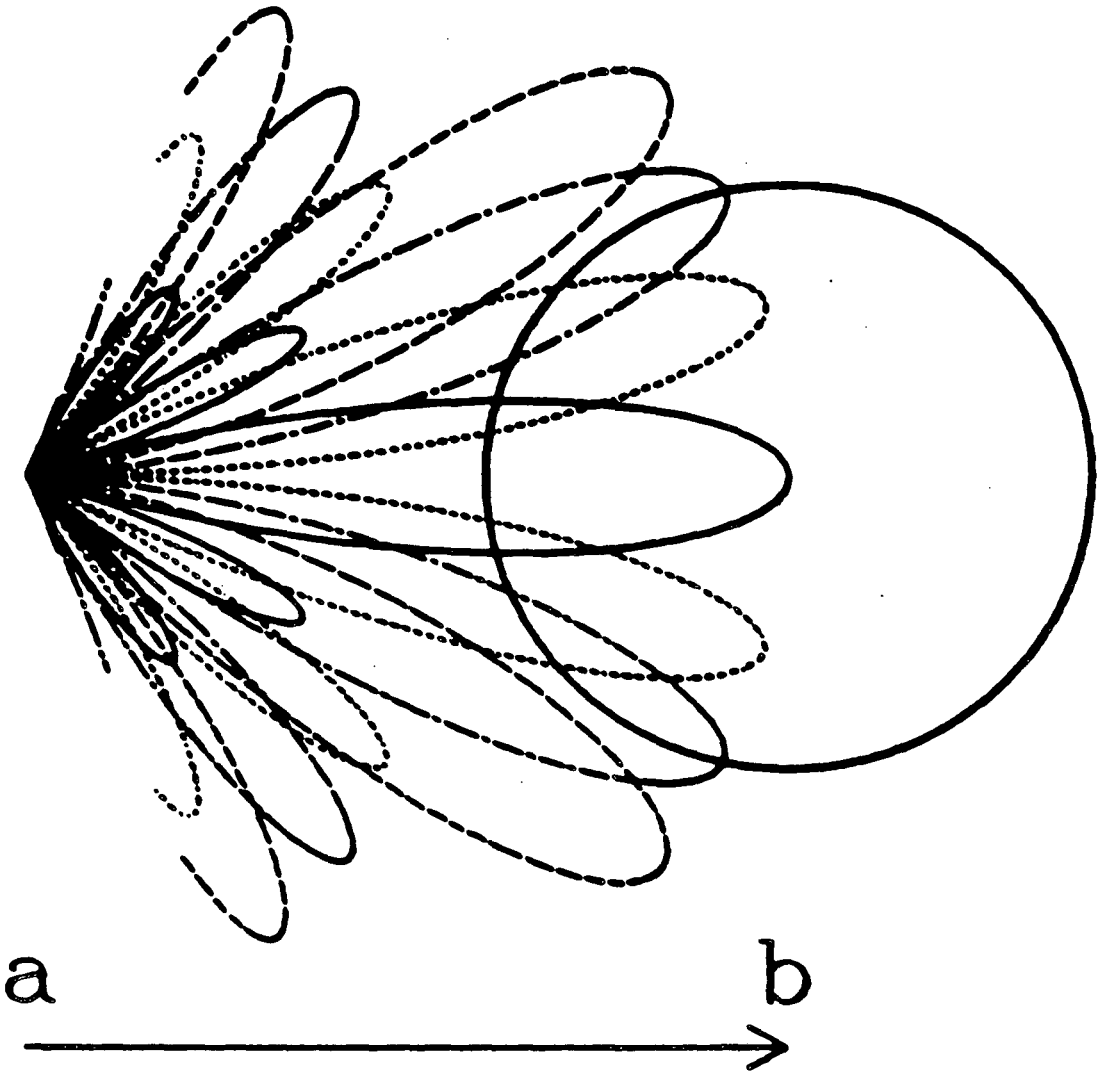

XBL 851-1019A

Figure 9

This report was done with support from the Department of Energy. Any conclusions or opinions expressed in this report represent solely those of the author(s) and not necessarily those of The Regents of the University of California, the Lawrence Berkeley Laboratory or the Department of Energy.

Reference to a company or product name does not imply approval or recommendation of the product by the University of California or the U.S. Department of Energy to the exclusion of others that may be suitable.

TECHNICAL INFORMATION DEPARTMENT
LAWRENCE BERKELEY LABORATORY
UNIVERSITY OF CALIFORNIA
BERKELEY, CALIFORNIA 94720